UNIVERSITY OF LEEDS

This is a repository copy of *Protein disulfide isomerase modulation of TRPV1 controls heat hyperalgesia in chronic pain*.

White Rose Research Online URL for this paper:
https://eprints.whiterose.ac.uk/185653/

Version: Published Version

Article:

White Rose
university consortium
Universities of Leeds, Sheffield & York

eprints@whiterose.ac.uk
https://eprints.whiterose.ac.uk/

Protein disulfide isomerase modulation of TRPV1 controls heat hyperalgesia in chronic pain

Graphical abstract

Highlights

- Nociceptive DRG neurons secret PDI, which is enhanced during chronic pain

- PDI serves as an endogenous TRPV1 activator

- PDI activates TRPV1 through oxidation of extracellular cysteines of TRPV1

- PDI is a potential therapeutic target for chronic pain
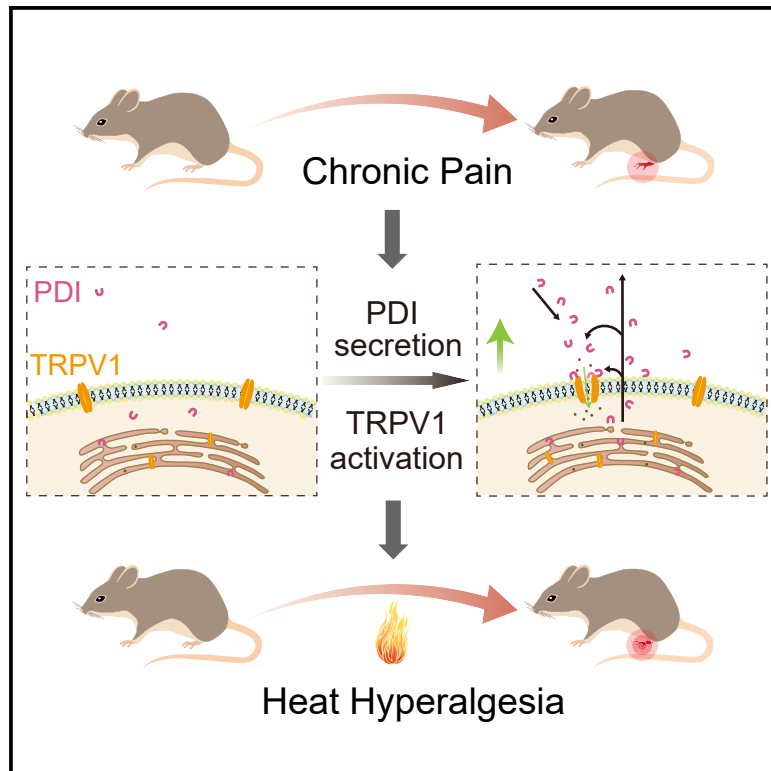
Authors

Yongxue Zhang, Qi Miao, Sai Shi, ...,
Yi Wu, Hailin Zhang, Xiaona Du

Correspondence

wuy@suda.edu.cn (Y.W.),
zhanghl@hebmu.edu.cn (H.Z.),
duxiaona@hebmu.edu.cn (X.D.)

In brief

Zhang et al. show upregulation of expression and secretion of PDI in dorsal root ganglion neurons in chronic pain conditions. Secreted PDI acts as endogenous TRPV1 activator by catalytic oxidation of extracellular cysteines of the channel, which is relevant to the development of heat hyperalgesia in chronic pain.

CelPress

Article

Protein disulfide isomerase modulation of TRPV1 controls heat hyperalgesia in chronic pain

Yongxue Zhang,[1,6] Qi Miao,[1] Sai Shi,[2] Han Hao,[1] Xinmeng Li,[1] Zeyao Pu,[1] Yakun Yang,[1] Hailong An,[2] Wei Zhang,[3] Youzhen Kong,[1] Xu Pang,[1] Cunyang Gu,[7] Nikita Gamper,[1,4] Yi Wu,[5,*] Hailin Zhang,[1,*] and Xiaona Du[1,8,*]

[1]Department of Pharmacology, The Key Laboratory of Neural and Vascular Biology, Ministry of Education, The Key Laboratory of New Drug Pharmacology and Toxicology, Hebei Medical University, Shijiazhuang, Hebei, China
[2]Key Laboratory of Molecular Biophysics, Institute of Biophysics, School of Science, Hebei University of Technology, Tianjin, China
[3]Department of Spinal Surgery of the Third Hospital of Hebei Medical University, Shijiazhuang, Hebei, China
[4]Faculty of Biological Sciences, University of Leeds, LS2 9JT Leeds, UK
[5]National Clinical Research Center for Hematologic Diseases, The First Affiliated Hospital, Cyrus Tang Medical Institute, Collaborative Innovation Center of Hematology, State Key Laboratory of Radiation Medicine and Prevention, Soochow University, Suzhou 215123, China
[6]Department of Pharmacy, The First Hospital of Handan, Handan, Hebei, China
[7]Department of Pathology, The Fourth Hospital of Shijiazhuang, Shijiazhuang, Hebei, China
[8]Lead contact
*Correspondence: wuy@suda.edu.cn (Y.W.), zhanghl@hebmu.edu.cn (H.Z.), duxiaona@hebmu.edu.cn (X.D.)
https://doi.org/10.1016/j.celrep.2022.110625

SUMMARY

Protein disulfide isomerase (PDI) plays a key role in maintaining cellular homeostasis by mediating protein folding via catalyzing disulfide bond formation, breakage, and rearrangement in the endoplasmic reticulum. Increasing evidence suggests that PDI can be a potential treatment target for several diseases. However, the function of PDI in the peripheral sensory nervous system is unclear. Here we report the expression and secretion of PDI from primary sensory neurons is upregulated in inflammatory and neuropathic pain models. Deletion of PDI in nociceptive DRG neurons results in a reduction in inflammatory and neuropathic heat hyperalgesia. We demonstrate that secreted PDI activates TRPV1 channels through oxidative modification of extracellular cysteines of the channel, indicating that PDI acts as an unconventional positive modulator of TRPV1. These findings suggest that PDI in primary sensory neurons plays an important role in development of heat hyperalgesia and can be a potential therapeutic target for chronic pain.

INTRODUCTION

Protein disulfide isomerase (PDI) was discovered by two independent research groups over 60 years ago (Goldberger et al., 1963; Venetianer and Straub, 1963). PDI is an abundant protein in the endoplasmic reticulum (ER), where its levels approach a millimolar range (Lyles and Gilbert, 1991), accounting for up to ~0.4% of total cellular protein (Hillson et al., 1984). PDI has a central role as a dithiol-disulfide oxidoreductase in catalyzing the reversible formation and isomerization of the disulfide bond (Wilkinson and Gilbert, 2004); PDI also acts as a molecular chaperone in ER (Ellis, 2013). PDI has an important physiological function to assist proper protein folding. It has also been implicated in several pathological conditions and diseases, particularly those related to ER stress and unfolded protein response (Matsusaki et al., 2020). For example, PDI upregulation was reported in many neurodegenerative diseases (Colla et al., 2012; Honjo et al., 2017; Massignan et al., 2007). It is believed that PDI upregulation is a protective response leading to a reduction in protein misfolding. However, long-term upregulation of PDI causes self-aggregation and may lead to oxidative stress (de A Paes et al.,

2011) and apoptosis (Hoffstrom et al., 2010). While the physiological and pathological functions of PDI in the CNS are under intense scrutiny, the functions of PDI in the peripheral nervous system are underexplored.

PDI has a multiple-domain structure that can be described as a-b-b'-x-a'-c (Wang et al., 2013); the active sites with CGHC motifs are located in the thioredoxin-like a and a' domains, whereas the substrate binding is accomplished by the b and b' domains. The x-linker is located between the a' and b' domains, whereas the C-terminal c domain carries a classic ER-retrieval signal sequence, KDEL (Pirneskoski et al., 2004). Despite the presence of the KDEL sequence, a small amount of PDI can still be secreted into the extracellular space and on the outer cell surface (Araujo et al., 2017; Furie and Flaumenhaft, 2014). Multiple redox-modulated targets have been described to be modulated by peri/epicellular PDI pools, including $\alpha_v\beta_3$ integrin in endothelial cells (Swiatkowska et al., 2008), tissue factor (Reinhardt et al., 2008), and $\alpha_{IIb}\beta_3$ in platelets (Lahav et al., 2002). PDI has also been reported to be detected in the cerebrospinal fluid (CSF) of amyotrophic lateral sclerosis (ALS) patients (Perri et al., 2017). In the CNS of rats, PDI expression was reported in
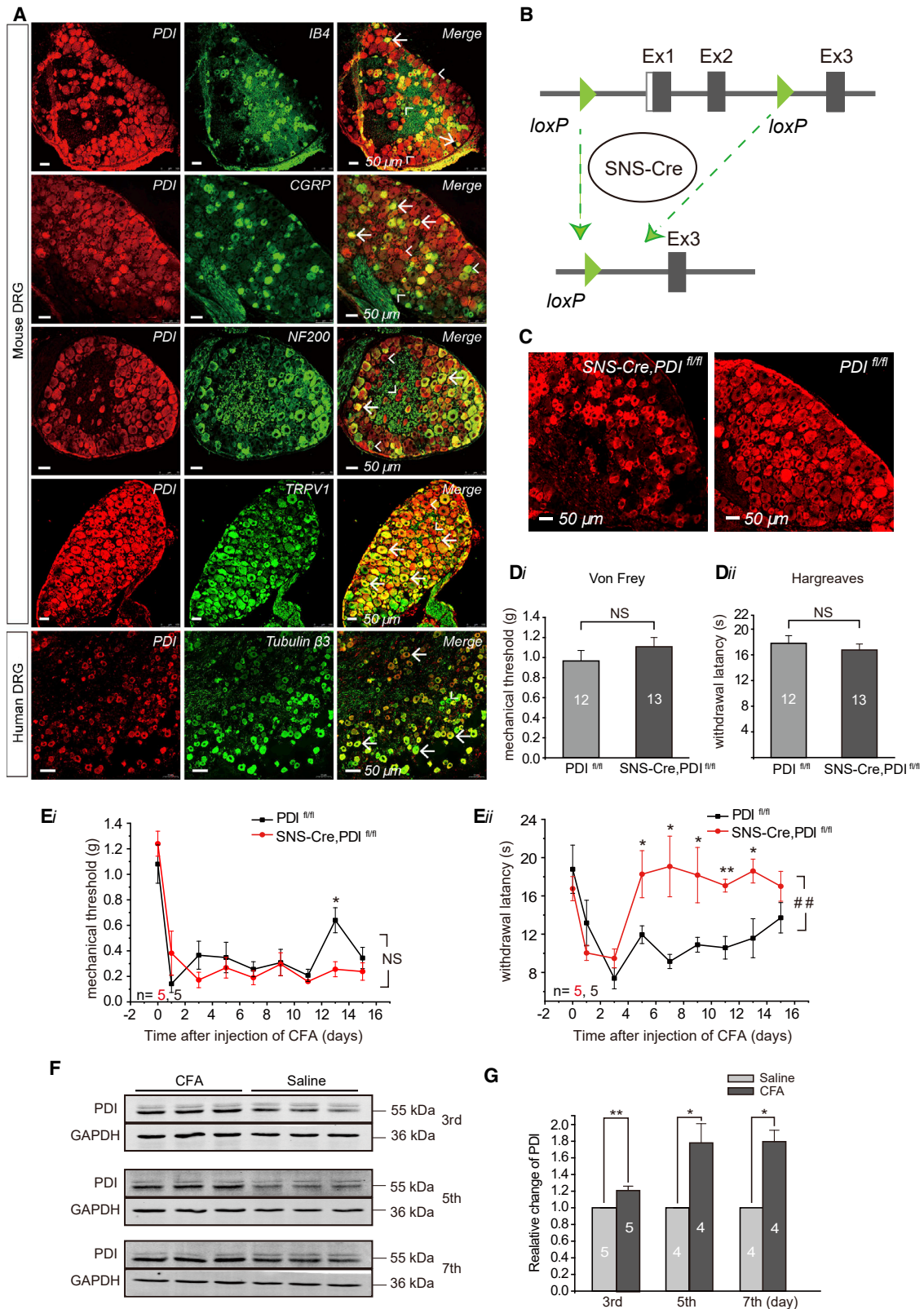
(legend on next page)

CA1-CA3 pyramidal cells and dentate granule cells (Kim et al., 2017). It was further reported that PDI potentiated seizure activity via the redox modulation of NMDA receptors, presumably via thiol modification of NR1 and NR2A subunits of the NMDA receptors in the ER and on the cell surface. Furthermore, PDI neutralization by a specific PDI antibody suppressed seizure activity (Kim et al., 2017). However, thus far, there is no direct evidence that PDI can be secreted in the nervous system.

Chronic pain is a complex disease with limited treatment approaches. Dorsal root ganglia (DRG) neurons are somatosensory neurons that innervate the skin, muscles, and visceral organs to detect various stimuli (chemical, thermal, or mechanical), including tissue injury and inflammation. Many ion channels, receptors, and signaling proteins in DRG neurons have been shown to be involved in chronic pain generation (Basbaum et al., 2009; Basso and Altier, 2017; Du et al., 2014, 2017; Moran and Szallasi, 2018). Our previous studies demonstrated that DRG plays an important role in somatosensory signal integration and represents an underappreciated "gate" for nociception transmission. Therefore, DRG offers a potential therapeutic target for chronic pain treatment (Du et al., 2014, 2017). Using data-independent acquisition-mass spectrometry analysis, it is reported that PDI protein is significantly upregulated in DRG neurons of mice with chronic inflammatory pain induced by complete Freund's adjuvant (CFA) injection (Rouwette et al., 2016). These findings also suggest the anti-algesic efficacy of a PDI inhibitor in a murine inflammatory pain model. However, a mechanistic understanding of the role of PDI in peripheral somatosensory nerves, particularly in relation to chronic pain development, is currently lacking.

In this study, we report that PDI expressed in DRG neurons is essential for the generation of heat hyperalgesia in chronic inflammation and neuropathic nerve injury; PDI could be secreted from DRG neurons, particularly under pathological conditions, and the secreted PDI functions as an endogenous algogen, which directly activates or sensitizes TRPV1 channels through extracellular cysteine oxidation.

RESULTS

PDI in the nociceptive DRG neurons selectively modulates heat hyperalgesia in chronic pain

PDI expression in DRG has been detected using an unbiased proteomics method (Rouwette et al., 2016). Here, we confirmed that PDI abundantly expressed in a majority of mouse DRG neurons (Figure 1A) using immunohistochemical analysis, with a relatively homogeneous distribution in DRG neuron subtypes, including neurons positive for isolectin B4 (IB4; non-peptidergic neurons), calcitonin gene-related peptide (CGRP; peptidergic neurons), and neurofilament-200 (NF200; myelinated neurons). We also tested PDI immunoreactivity in human DRG neurons and verified substantial PDI expression in human DRG neurons (Figure 1A, lower panel). To assess the potential role of PDI in nociception, we generated a mouse line with conditional deletion of PDI in somatosensory neurons expressing Nav1.8 channel, which is a nociceptor-specific Na^+ channel (Agarwal et al., 2004; Zhou et al., 2015) (Figure 1B). PDI expression was markedly reduced in the DRG of SNS-Cre, $PDI^{fl/fl}$ mice as determined by immunofluorescence assay (Figure 1C).

The sensitivities of SNS-Cre, $PDI^{fl/fl}$ mice to mechanical and heat stimuli were measured. Compared with the control $PDI^{fl/fl}$ mice, the SNS-Cre, $PDI^{fl/fl}$ mice showed no significant differences in basal response thresholds to either mechanical (Figure 1Di) or heat (Figure 1Dii) stimuli. For thermosensation, we also demonstrated that SNS-Cre, $PDI^{fl/fl}$ and control ($PDI^{fl/fl}$) mice showed no differences responding to a range of noxious temperature stimuli using a hot plate test (Figure S1A) and tail-flick test (Figure S1B). These results suggest that PDI deletion in Nav1.8-positive DRG neurons does not affect basal sensitivity to noxious stimuli.

Next, we tested if and how PDI deletion affected the development of chronic inflammatory pain. We used the CFA model of chronic inflammation. CFA was injected into the right hind paw of either control ($PDI^{fl/fl}$) or PDI knockout (SNS-Cre, $PDI^{fl/fl}$) mice, and behavioral tests were performed every second day for 14 days after the CFA injection. As expected, CFA injection induced robust mechanical and heat hyperalgesia in the control $PDI^{fl/fl}$ mice (Figure 1E); in the SNS-Cre, $PDI^{fl/fl}$ mice injected with CFA, the mechanical withdrawal thresholds were comparable to the $PDI^{fl/fl}$ mice (Figure 1Ei), whereas their heat withdrawal latencies were significantly increased in comparison with the $PDI^{fl/fl}$ mice (Figure 1Eii). We also performed similar behavioral tests in a neuropathic pain model of chronic constriction injury (CCI). Similar to the above inflammatory pain model, the SNS-Cre, $PDI^{fl/fl}$ mice after CCI operation also demonstrated significantly attenuated heat hyperalgesia but maintained a similar level of mechanical hyperalgesia as the $PDI^{fl/fl}$ control mice (Figures S1C and 1D). Similar to the CFA model, in the first 4 days after injury, heat hyperalgesia developed with similar kinetics in both the $PDI^{fl/fl}$ and SNS-Cre, $PDI^{fl/fl}$ mice; however, in

Figure 1. PDI in DRG neurons is required for chronic heat hyperalgesia

(A) Immunofluorescence of PDI expression in mouse and human DRG neurons. In mouse DRG sections: co-localization of PDI with DRG neuron markers IB4, CGRP, and NF200. Arrows indicate examples of co-localization of PDI and DRG neuron markers, arrowheads indicate only expression of PDI. In human DRG section: tubulin β3 staining labels all neurons. Arrows indicate examples of PDI-positive DRG neurons and arrowheads indicate PDI-negative DRG neurons. Scale bars, 50 μm.

(B) Diagram depicts the generation of the SNS-Cre,$PDI^{fl/fl}$ mice.

(C) Immunofluorescence shows PDI expression in DRG neurons in the SNS-Cre,$PDI^{fl/fl}$ mice is decreased in comparison with the $PDI^{fl/fl}$ mice.

(Di) Nocifensive response to mechanical stimulation. (Dii) Nocifensive response to radiant heat.

(Ei) Mechanical thresholds in the inflammatory CFA model. (Eii) Withdrawal latencies in the inflammatory CFA model (repeated measures ANOVA, # #p < 0.01, Student's t test or Mann-Whitney U test was used for test difference between two groups within the corresponding time point, *p < 0.05, **p < 0.01).

(F) Western blot results of PDI protein in the DRG of mice subjected to CFA treatments.

(G) Summary for (F), one-sample t test. *p < 0.05, **p < 0.01. Numbers in bar graphs represent experimental repetitions. Data are represented as mean ± SEM. See also Figure S1.

the PDI knockout mice, the withdrawal latency did not reach the same hyperalgesic levels as in the control animals and stopped declining at later time points. These results suggest that PDI expressed in DRG neurons plays a crucial role in developing heat hyperalgesia in chronic pain.

One hypothesis that would explain the reduced heat hyperalgesia after the knockout of PDI from nociceptors is an increased activity of PDI during the development of heat hyperalgesia. To test this hypothesis, we first measured the protein expression levels of PDI in the DRG of CFA-injected wild-type (WT) mice. CFA or saline was injected into the right and left hind paws of the mice, respectively. As significant mechanical and heat hyperalgesia occurred from the third day after CFA injection, we extracted both sides of the L3-L5 DRG from the mice on the third, fifth, and seventh days after CFA injection for western blot analysis. The PDI protein levels were elevated in the CFA-treated side DRGs (Figures 1F and 1G). Similarly, significant upregulation of PDI proteins was also observed in CCI-treatment side of L3-L5 DRGs of the mice on the fifth, seventh, and 10th days after surgery, compared with the contralateral side of DRG (Figures S1E and S1F).

Next we tested whether the chronic pain-induced increase in PDI expression in the DRG was accompanied by an increase in its secretion. L3-L5 DRGs of WT mice were disassociated and incubated with either PDI antibody or control immunoglobulin (Ig)G without permeabilization, and cell surface PDI antibody labeling of cells was analyzed using flow cytometry. This experiment evaluated the secreted PDI, which is being retained on the surface of the DRG cells. As shown in Figure S2A, DRG cells incubated with PDI antibody exhibited significantly higher fluorescence intensity than IgG control, implying the presence of PDI proteins on the surface of DRG cells. We performed similar experiments on mice treated with the CFA injection. The results in Figure S2B show that CFA injection induced significant upregulation of PDI on the outer surface of the DRG cells, compared with saline-injected controls. We also tested the release of PDI by DRG cells using an ELISA assay, which measured the PDI concentration in the extracellular solution bathing the DRG tissue and found that the release of PDI was also increased by CFA treatment (Figure S2C). This CFA-induced increase in PDI release was only seen in the DRG from the control PDI$^{fl/fl}$ mice, but not in those from the SNS-Cre, PDI$^{fl/fl}$ mice (Figure S2Cii). These results suggest that PDI is expressed in DRG neurons and is secreted onto the cell surface and into the extracellular space of the DRG neurons; the expression and secretion of PDI by DRG neurons was significantly upregulated in the chronic inflammatory condition.

PDI directly activates TRPV1 channel and excites the nociceptive DRG neurons

The selective effect of PDI deletion on heat hypersensitivity led us to speculate that PDI might directly modulate thermosensitive TRPV1 channels (Tominaga et al., 1998). To explore this possibility, we first investigated whether a purified PDI would invoke TRPV1-dependent nocifensive behavior. We prepared recombinant human PDI (hPDI) and its catalytically inactivated recombinant (hPDIoooo) (Zhou et al., 2015). The purity and functionality of these recombinant proteins were tested by SDS-PAGE and

Di-E-GSSG reduction assay; ~90% purity was achieved (Figure S3A) and the purified recombinant hPDI proteins showed full reductase activity, whereas the hPDIoooo showed no such activity (Figure S3B).

We then injected purified hPDI or hPDIoooo into the right hind paw of WT mice, and spontaneous nocifensive behaviors were observed for 30 min; a group of WT mice injected with saline was used as control (Figure 2A). Intraplantar injection of hPDI induced robust nocifensive behaviors, which were significantly more pronounced compared with the responses to either saline or hPDIoooo injections; no difference was found for the latter two groups. Thereafter, we tested the algogenic effect of hPDI on TRPV1 knockout (TRPV1-KO) mice. TRPV1-KO mice did not display elevated nocifensive behavior in response to hPDI injection, whereas their WT littermates did (Figure 2B). These results indicate that PDI modulation of TRPV1 may contribute to the heat hyperalgesia observed in pathological chronic pain conditions.

To obtain more direct evidence for PDI modulation of TRPV1, we tested the effects of PDI on TRPV1 function using electrophysiology. First, purified recombinant hPDI was tested for its effects on TRPV1-mediated membrane currents. In the isolated cultured small-diameter (15–25 μm) presumed nociceptive DRG neurons; hPDI, but not hPDIoooo, induced inward depolarizing currents recorded with whole-cell patch clamp at a holding potential of – 60 mV (Figure 2C, room temperature). In addition, the hPDI-induced inward depolarizing currents were significantly reduced in the presence of the TRPV1 blocker capsazepine (Figure 2D) and markedly reduced in the DRG neurons from TRPV1-KO mice (Figure 2E). These experiments indicate that PDI-induced currents are mainly mediated by endogenous TRPV1 in DRG neurons. Furthermore, hDPI but not hPDIoooo increased the frequency of action potential (AP) firing (Figures S4A and S4B) and depolarized the membrane potential of the DRG neurons (Figure S4C).

To further prove that the TRPV1 channel is the direct target for PDI action, we studied the effect of PDI on the TRPV1 channels heterologously expressed in HEK293 cells. We first tested mouse TRPV1 (mTRPV1), as this study used a mouse model. Extracellular application of hPDI but not hPDIoooo, evoked a robust inward current in HEK293 cells expressing mTRPV1 (Figure 2Fi), which was similar to the PDI-induced inward currents observed in the cultured DRG neurons, with only a larger current amplitude. Since we used hPDI, we also tested the effects of hPDI on human TRPV1. Similar to mTRPV1, human TRPV1 (hTRPV1) expressed in HEK293 cells also responded to hPDI with robust inward currents (Figure 2Fii). No visible currents were induced by hPDI in untransfected HEK293 cells (data not shown). These results further identified TRPV1 as a direct target of PDI activation.

Mechanism for PDI modulation of TRPV1

The above results suggest that PDI could directly activate the TRPV1 channel. However, considering the central role of PDI in assisting protein folding (Hillson et al., 1984; Wilkinson and Gilbert, 2004), we investigated whether PDI could also modulate the proper TRPV1 expression. Thus, we tested TRPV1 expression levels in the DRG from PDI knockout mice (SNS-Cre,
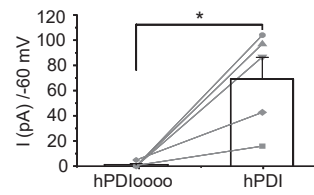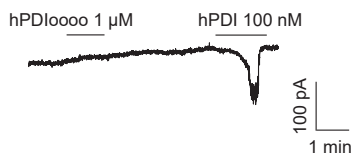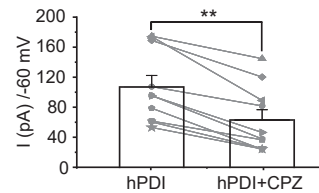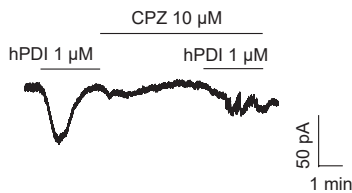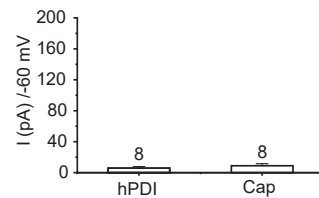
A WT
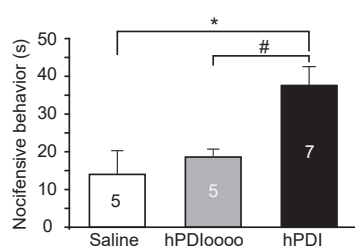
B TRPV1-KO
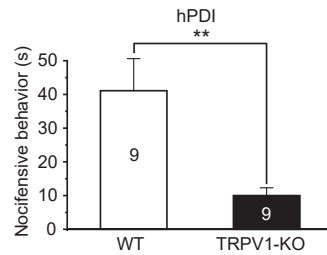
C DRG neurons/WT
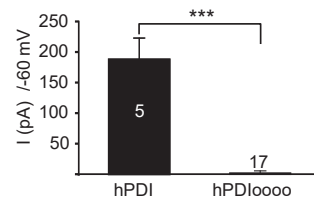

D DRG neurons/WT

E DRG neurons/TRPV1-KO
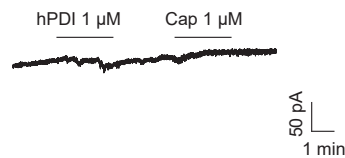
F HEK293/TRPV1

i. mTRPV1
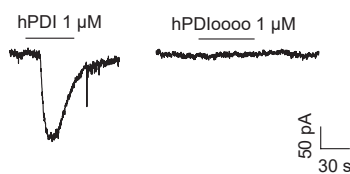
ii. hTRPV1
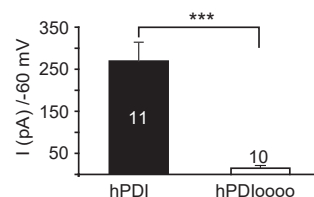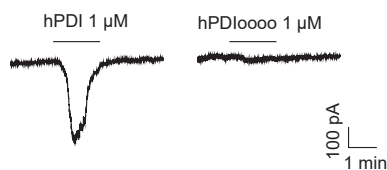
Figure 2. TRPV1 mediates the PDI-induced heat hyperalgesia and is activated by PDI

(A) Intraplantar injection of hPDI, but not the inactive mutant hPDIoooo, induced nocifensive behaviors in the WT mice (one-way ANOVA followed by Student-Newman-Keuls test, * #p < 0.05).

(B) Knockout of TRPV1 significantly reduced the nocifensive behaviors induced by intraplantar injection of hPDI (Mann-Whitney *U* test, **p < 0.01).

(C) hPDI but not hPDIoooo induced inward currents in the disassociated DRG neurons (paired t test, *p < 0.05).

(D) TRPV1 antagonist capsazepine (CPZ) significantly reduced the hPDI-induced inward currents (paired t test, ***p < 0.001).

(E) The hPDI-induced currents were totally abolished in DRG neurons of TRPV1-KO mice.

(F) hPDI but not hPDIoooo activated both mice TRPV1 (mTRPV1) (i) and human TRPV1 (hTRPV1) (ii) (Mann-Whitney *U* test, ***p < 0.001). Numbers in bar graphs represent experimental repetitions. Data are represented as mean ± SEM.

Figure 3. Selective deletion of PDI in nociceptive DRG neurons does not affect the expression and function of TRPV1

(A) Immunofluorescence results of TRPV1 in DRG slices from the control (PDI^{fl/fl}) and the nociceptive DRG neuron-TRPV1-deleted (SNS-Cre, PDI^{fl/fl}) mice. Scale bars, 50 μm.

(B) Western blot results for the expression of TRPV1 and PDI in DRG tissue of the PDI^{fl/fl} and the SNS-Cre, PDI^{fl/fl} mice in (Bi); normalized expression level is shown in (Bii) (one-sample t test, *p < 0.05).
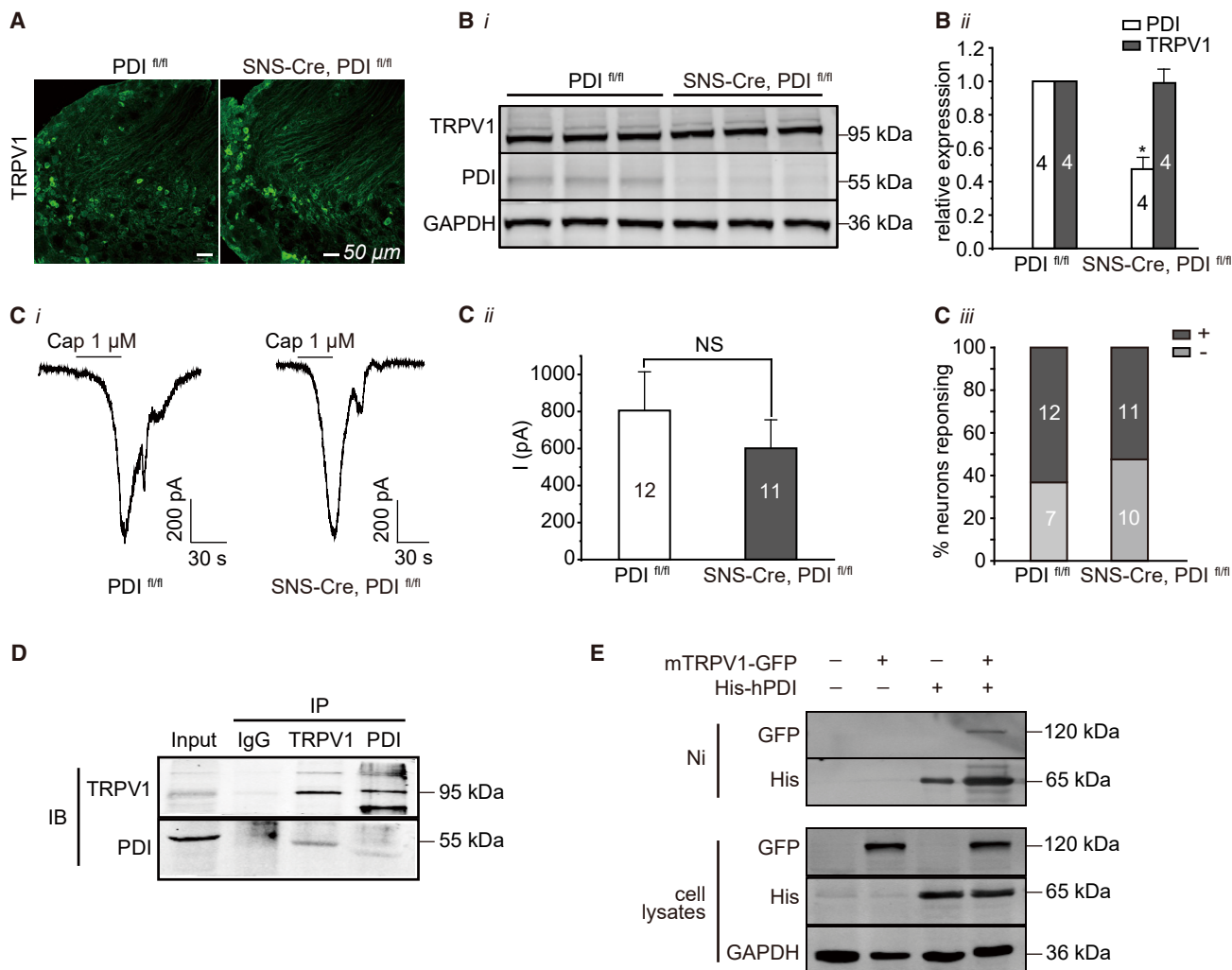
(C) Capsaicin-induced TRPV1 currents in disassociated DRG neurons (i, whole-cell currents from holding potential of −60 mV) were not affected by selective deletion of PDI in the nociceptive DRG neurons (ii, Mann-Whitney U test, p > 0.05); percentage of DRG neurons responding (black colored) to capsaicin with measurable inward currents were not significantly different between the control and the PDI-deleted neurons (iii, chi-square test, p > 0.05).

(D) Immunoprecipitating results showing the interaction between TRPV1 and PDI in the DRG.

(E) Pull-down results showing the interaction between the expressed mTRPV1 and hPDI in HEK293 cells. Numbers in bar graphs represent experimental repetitions. Data are represented as mean ± SEM.

PDI^{fl/fl}). Immunofluorescence (Figure 3A) and western blotting (Figure 3B) suggested that PDI deletion did not significantly affect TRPV1 levels in the DRG. Furthermore, the TRPV1 current amplitudes and the proportion of TRPV1-responsive neurons to 1 μM capsaicin were not affected by selective deletion of PDI in nociceptive DRG neurons (Figure 3C). Lower concentrations of capsaicin (0.5 and 0.25 μM) were also tested, and no differences were observed in PDI CKO neurons in comparison with controls (data not shown). These results indicate that PDI does not affect TRPV1 expression and function under normal physiological con-

ditions, in line with the findings that mice with selective deletion of PDI in nociceptive DRG neurons exhibited normal sensitivity to heat (Figure 1Dii).

Next, we tested the possible interactions between PDI and TRPV1. First, immunoprecipitation was performed in DRG tissue from WT mice and it was found that PDI and TRPV1 could co-immunoprecipitate with each other (Figure 3D). We then co-transfected GFP-tagged mTRPV1 and His-tagged hPDI into HEK293 cells and confirmed that GFP-tagged mTRPV1 was co-purified with His-tagged hPDI on a Ni column (Figure 3E).
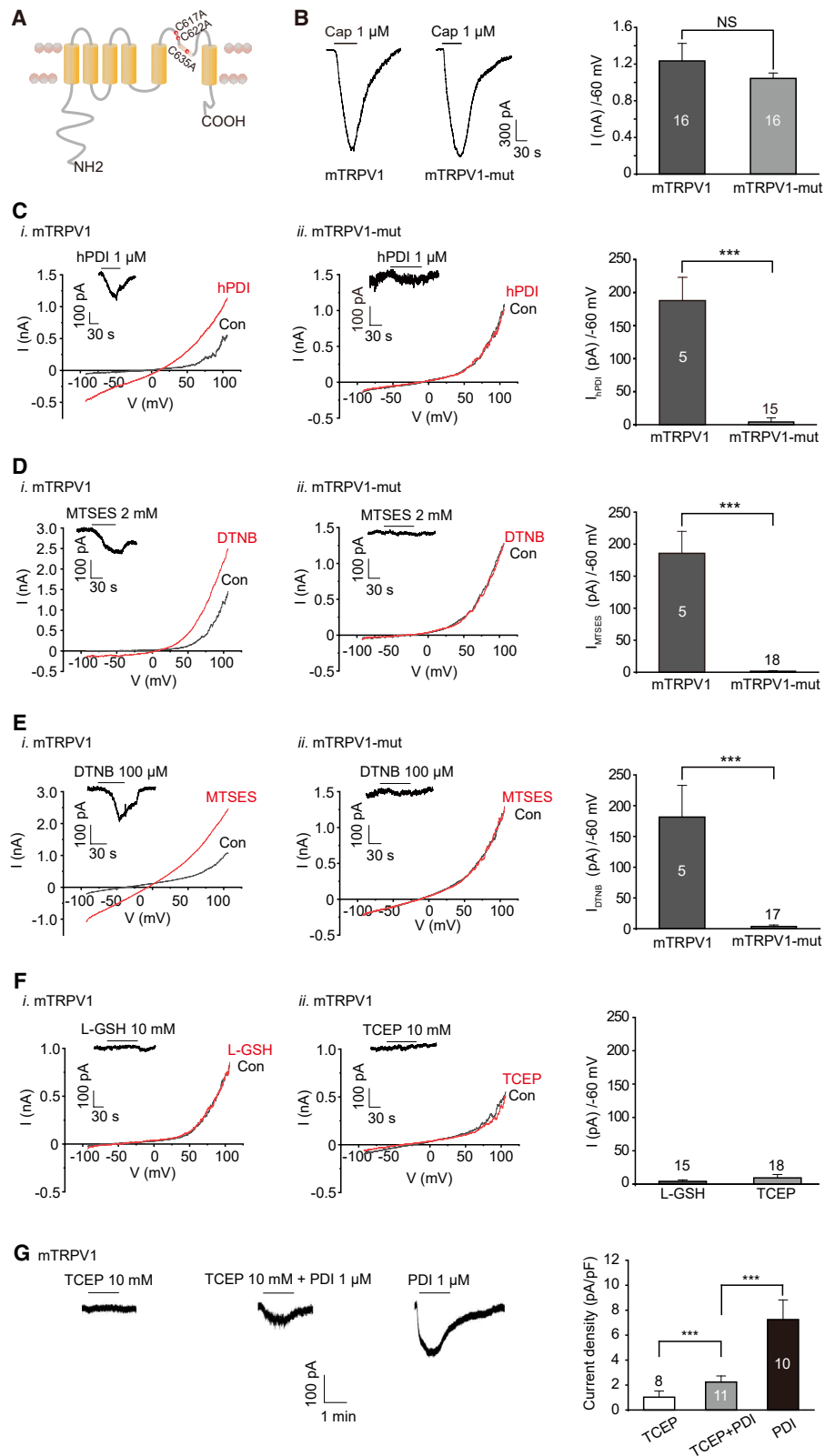
The results so far suggest a direct activation or sensitization of TRPV1 by PDI in chronic pain conditions, presumably due to the increased excretion of PDI and subsequently enhanced interactions between PDI and TRPV1 in these pathophysiological conditions. We next explored putative molecular mechanisms underlying the action of PDI on TRPV1. Since PDI catalyzes the thiol-disulfide interchange reactions between cysteines, the cysteines within the TRPV1 protein were studied for their possible involvement in PDI action. Since PDI excretion is increased in chronic pain states, we focused on a potential extracellular site of action. The mTRPV1 channel contains three extracellular cysteines: C617, C622, and C635. It has been reported that C617 and C622 are located in the pore turret and are important for the heat activation of the channel (Yang et al., 2010). Accordingly, we generated an mTRPV1 mutant with all three cysteine residues substituted by alanines (mTRPV1-mut; C617A, C622A, and C635A, Figure 4A) and tested its response to PDI in HEK293 cells. Capsaicin activated mTRPV1 and mTRPV1-mut similarly (Figure 4B), indicating that the mutation did not affect TRPV1 gating by capsaicin and did not significantly affect the membrane expression of the channel. However, whereas hPDI robustly activated mTRPV1, it failed to activate TRPV1-mut completely (Figure 4C).

We also performed similar experiments on hTRPV1. hTRPV1 has only two cysteines (C621 and C635) in the extracellular domain (Figure S5A). Similar to mTRPV1, mutation of these two cysteines in hTRPV1 (hTRPV1-mut, C621A, and C635A) did not affect its response to capsaicin (Figure S5B) but completely abolished its response to hPDI (Figure S5C). These results indicate that these extracellular cysteines in TRPV1 are crucial sites for the PDI activation of TRPV1.

It is known that PDI has both oxidized and reduced states in solution (Okumura et al., 2019); thus, we next investigated whether an oxidizing or reducing reaction of these cysteines in TRPV1 contributes to the activation of TRPV1. We used membrane-impermeable oxidants and reductants to test their effects on the TRPV1 channel and its mutants expressed in HEK293 cells, to observe which of these would affect TRPV1 in a manner similar to that of PDI. MTSES (sodium (2-sulfonatoethyl) methane thiosulfonate) is a membrane-impermeable oxidative reagent commonly used to covalently modify the cysteine side chains of the proteins (Pan et al., 2018). MTSES applied extracellularly, effectively activated mTRPV1; however, it had little effect on mTRPV1-mut (Figure 4D). Another membrane-impermeable oxidant, DTNB (5,5′-dithio-bis-nitrobenzoic acid) (Chuang and Lin, 2009) similarly activated mTRPV1 but not the mTRPV1-
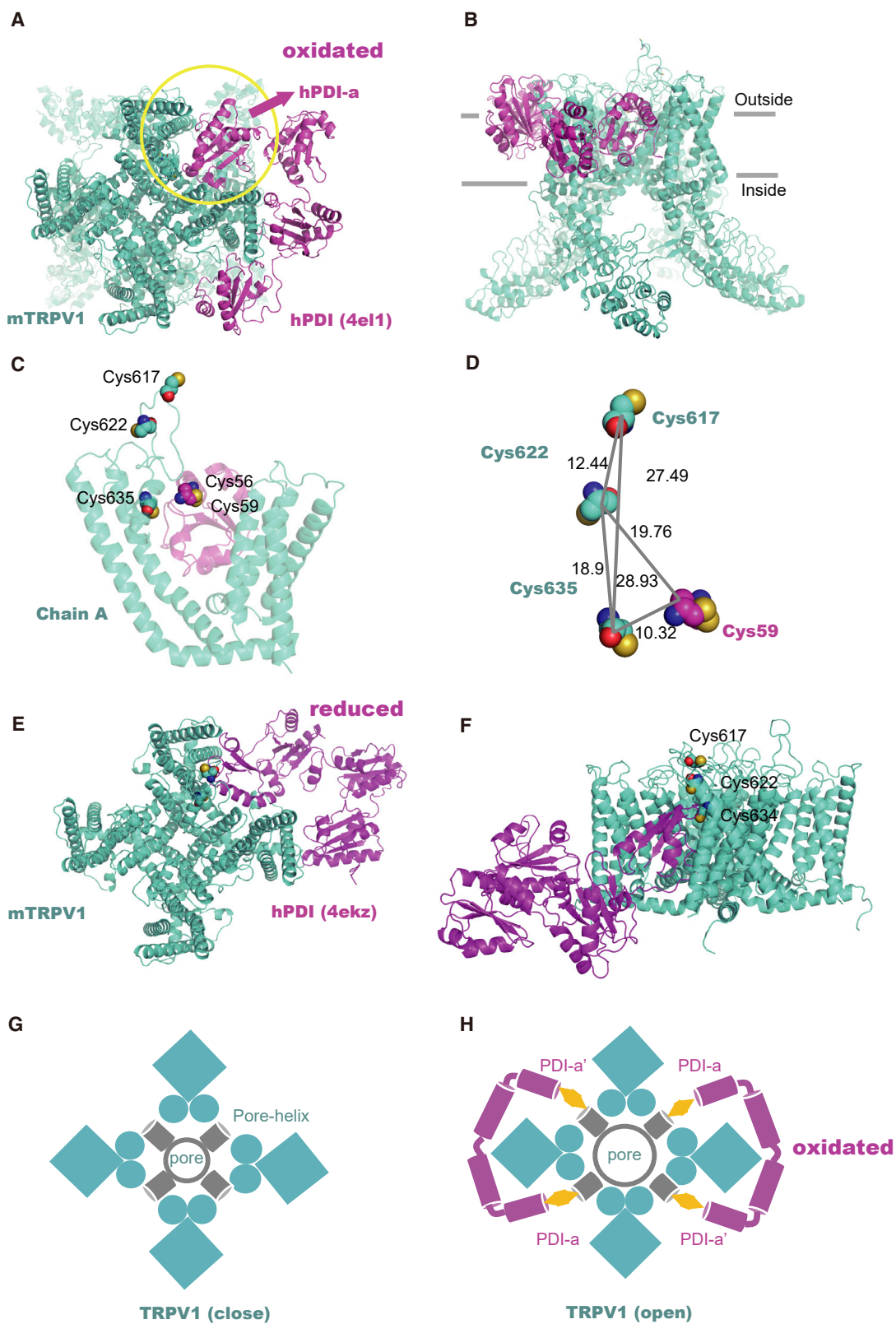
mut (Figure 4E). In contrast, when two membrane-impermeable reductants, L-GSH (reduced glutathione) (Susankova et al., 2006) and TCEP (Tris (2-carboxyethyl) phosphine) (Grand et al., 2018; Li et al., 2019), were applied extracellularly at 10 mM, no activation of mTRPV1 was observed (Figure 4F). Next we applied the reductant TECP together with PDI in the extracellular solution to test its effect on mTRPV1 current. Although there is still a small current, TECP applied with PDI dramatically reduced the ability of PDI to activate mTRPV1 (Figure 4G). This result suggests that PDI activates TRPV1 through oxidative reaction. We also tested these chemical reagents on hTRPV1 and its mutant (hTRPV1-mut) (Figures S5D–S5F); the results were similar to mTRPV1: the oxidants (MTSES and DTNB) activated hTRPV1 but not hTRPV1-mut; the reductants (L-GSH and TCEP) did not activate hTRPV1. These results suggest that both mTRPV1 and hTRPV1 are in a functional state that can be modified by oxidative but not reducing reactions, and the oxidative reaction is likely mediated by the extracellular cysteines in TRPV1.

Molecular structural simulation of interaction between hPDI and TRPV1

To gain a deeper insight into the potential mechanism for PDI activation of mTRPV1 at the molecular level, we simulated the molecular dynamic interactions between PDI and TRPV1. The resolved hPDI structures include reduced (PDB: 4ekz) and oxidized (PDB: 4el1) states (Wang et al., 2013). The resolved rTRPV1 structure lacks the region of 604–626 because of its highly divergent property (Cao et al., 2013), and this missing region unfortunately includes the C617 and C622 in mTRPV1 (C616 and C621 in rTRPV1). Therefore, we first constructed a simulated structure of whole-length mTRPV1 using homology modeling based on the rTRPV1 structure (PDB: 3j5p), which is in a closed state. Thereafter, we performed computational molecular docking between the constructed mTRPV1 and the different structural states of hPDI. As shown in Figure 5A, the mTRPV1 channel has a tetrameric architecture, and the four subunits are arranged in 4-fold symmetry around the central ion permeation pathway. The oxidized hPDI has an opened structure with a "U" shape (Wang et al., 2013). Docking simulation positioned the oxidized hPDI embracing the mTRPV1 channel from outside, with two active domains of oxidized hPDI interacting with two adjacent subunits of the mTRPV1 channel (Figures 5A and 5B). The high-resolution simulated structure shows that C617 and C622 residing in the extracellular loop and C635 located in the S5-S6 helix of the mTRPV1 channel, and C56 or C59 (C53 or C56 in original protein sequence) in the active site

Figure 4. PDI and oxidants activate TRPV1 through extracellular cysteine residues
(A) Topology diagram of mTRPV1 with the indicated mutated extracellular cysteines (mTRPV1-mut).
(B) Mutation of the extracellular cysteines did not affect capsaicin (Cap)-induced activation of mTRPV1. Exemplary and summarized mTRPV1 and mTRPV1-mut currents induced by Cap at holding potential of −60 mV are shown.
(C) Whole-cell currents of mTRPV1 and mTRPV1-mut were recorded either under a constant −60 mV holding potential (inset) or a ramp holding potential from −100 mV to +100 mV (800 ms). The current amplitudes recorded at −60 mV are summarized and analyzed (Mann-Whitney *U* test, ***p < 0.001).
(D–F) Exemplary and summarized mTRPV1 currents induced by the oxidants MTSES (D), DTNB (E), and the reductants L-GSH (Fi), TCEP (Fii). The oxidants activated mTRPV1 but not mTRPV1-mut channels; the reductants did not activate mTRPV1 channels (Mann-Whitney *U* test, ***p < 0.001).
(G) Exemplary and summarized mTRPV1 currents induced by TECP, TCEP + PDI, and PDI. TCEP + PDI significantly diminishes PDI effect on the current (Mann-Whitney *U* test, ***p < 0.001). Numbers in bar graphs represent experimental repetitions. Data are represented as mean ± SEM.
See also Figure S5.

A

oxidated

hPDI-a

mTRPV1   hPDI (4el1)

B

Outside

Inside

C

Cys617

Cys622

Cys56
Cys635   Cys59

Chain A

D

Cys622   Cys617

12.44   27.49

19.76

18.9   28.93

Cys635   10.32   Cys59

E

reduced

mTRPV1   hPDI (4ekz)

F

Cys617

Cys622

Cys634

G

Pore-helix

pore

TRPV1 (close)

H

PDI-a'   PDI-a

pore

oxidated

PDI-a   PDI-a'

TRPV1 (open)

(legend on next page)

of hPDI (*a* domain) are in very close proximity (Figures 5C and 5D), which provides a good chance of directly catalyzing the reaction of PDI on the TRPV1 channel. In contrast, the reduced hPDI displaying a relatively closed structure (Wang et al., 2013) could only interact with the mTRPV1 subunit via one of its active domains (Figures 5E and 5F). The simulation of the interactions between hPDI and hTRPV1 showed similar results (Figures S6). These simulations, together with the results obtained using hPDI and oxidants, suggest that the TRPV1 channel is likely to be regulated by the oxidized form of hPDI. Combining these simulations and the above electrophysiological results, we proposed a working model for the PDI activation of TRPV1 (Figures 5G and 5H). We suggest that cysteines at two active sites of oxidized hPDI interact with extracellular cysteines within TRPV1, which drives the conformational change of the TRPV1 channel from closed to open state.

Extracellular cysteines in TRPV1 are crucial for heat hyperalgesia in chronic pain states

In the next series of experiments, we aimed to establish a direct link between PDI modulation of TRPV1 via extracellular cysteines and hyperalgesia associated with chronic pain. We reasoned that it should be possible to "rescue" the reduced heat hyperalgesia observed in TRPV1-KO mice by re-expression in the DRG of the WT TRPV1 channel, but not the TRPV1-mut channel lacking the key cysteines. We obtained AAV9 viral constructs carrying mTRPV1 or mTRPV1-mut (C617A/C622A/635A) with EGFP (Figure 6A) and injected them into the L3 and L4 DRG of TRPV1-KO mice (see STAR Methods and Figure 6B); AAV 9 viruses carrying only EGFP were used as control. EGFP fluorescence was readily detectable in the L3 and L4 DRGs of the mice, 4 to 6 weeks after the virus injection (Figure 6C, left). Expression of mTRPV1 and mTRPV1-mut was verified using anti-TRPV1 antibodies (Figure 6C, middle). Functional expression of these TRPV1 channels was verified by studying their activation by capsaicin in disassociated DRG neurons expressing EGFP; as expected, no capsaicin-induced currents were observed in the control DRG neurons (TRPV1-KO transduced with EGFP, Figure 6D). These results demonstrated effective rescue of TRPV1 expression in the DRG of TRPV1-KO mice. The capsaicin-induced currents were comparable in amplitude in DRG neurons from both mTRPV1- and TRPV1-mut-expressing mice (Figure 6E), which is consistent with previous results showing that the substitution of extracellular cysteines in mTRPV1 does not affect the sensitivity of the channels to capsaicin (Figure 4B).

Thereafter, behavioral tests were performed to test whether functional restoration of TRPV1 in the DRG would render TRPV1-KO mice with nocifensive behavior to capsaicin and hPDI. Indeed, capsaicin induced robust nocifensive behaviors in TRPV1-KO mice overexpressing either mTRPV1 or mTRPV-mut. This was in stark contrast to the control virus-injected mice, which showed only marginal nocifensive response to capsaicin (Figure 6F). When the hPDI was injected into the hind paw instead of capsaicin, significant nocifensive behaviors were only observed in TRPV1-KO mice overexpressing mTRPV1 but not TRPV1-mut-expressing or GFP-expressing mice (Figure 6G). These results demonstrate that extracellular cysteines in TRPV1 are crucial for PDI-induced nocifensive behavior.

Inhibition of peripheral PDI alleviates heat hyperalgesia in chronic pain states

The evidence collected thus far indicates a role for PDI in pathophysiological rather than physiological nocifensive behavior; this presents PDI as a potential therapeutic target for pain control. To explore this possibility, we investigated whether blocking PDI in the periphery would alleviate chronic pain. First, we used intraplantar injection of anti-PDI antibody RL90 (Zhou et al., 2015) to block peripheral PDI activity. The effect of such injection on heat and mechanical hyperalgesia in CFA and CCI chronic pain models was examined. RL90 was pre-injected into the hind paw of mice 5 hours before the behavioral measurements on the fifth and 11th days after CFA injection or CCI surgery (Figure 7A). IgG was injected at the same time points as controls. As compared with IgG, there was a borderline reduction in mechanical hyperalgesia after the RL90 injections in both pain models; the effect only reached significance at some time points (Figures 7Bi and 7Ci). However, RL90 significantly relieved heat hyperalgesia at each time point of injection (the fifth and 11th days), in both CFA and CCI models, with significantly prolonged withdrawal latency to heat stimulation (Figures 7Bii and 7Cii) in comparison with IgG-injected mice. These results further support the idea that PDI is an important player in heat hyperalgesia in chronic pain.

Finally, we used a different strategy to block hPDI involvement in hyperalgesia in chronic pain: hPDIoooo, the hPDI mutant lacking the catalytic activity (Figure S3), was used as a competitive blocker of hPDI, which would antagonize the algogenic effect of hPDI. Indeed, hPDIoooo pre-injected into the hind paw significantly relieved the heat hyperalgesia on the fifth day in both CFA and CCI models (Figures 7D and 7E) but had no obvious effects on mechanical hyperalgesia (data not shown). These results suggest that PDI blocking is effective in alleviating heat hyperalgesia in chronic pain conditions.

Figure 5. Structural simulation and molecular docking between TRPV1 and hPDI
(A) Top view of the interaction between mTRPV1 (cyan) and hPDI (purple).
(B) Side view of the interaction and relative position between mTRPV1 and the oxidated hPDI (PDB: 4el1).
(C and D) The relative distance of Cys617, Cys622, Cys635 in mTRPV1 and Cys56, Cys59 in hPDI (PDB: 4el1).
(E) Top view of the interaction between mTRPV1 (cyan) and the reduced hPDI (purple, PDB: 4ekz).
(F) Side view of the interaction between mTRPV1 and hPDI (PDB: 4el1) in reduced state.
(G and H) Working models for PDI activation of TRPV1. (G) TRPV1 at close state. Four TRPV1 subunits (cyan) form a tetrameric architecture and the four pore helix (gray) are arranged in 4-fold symmetry around central ion permeation pathway. (H) A tetrameric TRPV1 (cyan) channel can interact with two "U"-shaped oxidated PDI (purple). Two active centers (a and a', yellow) of one oxidated PDI (purple) interact with two adjacent TRPV1 subunits and force the channel open.
See also Figure S6.
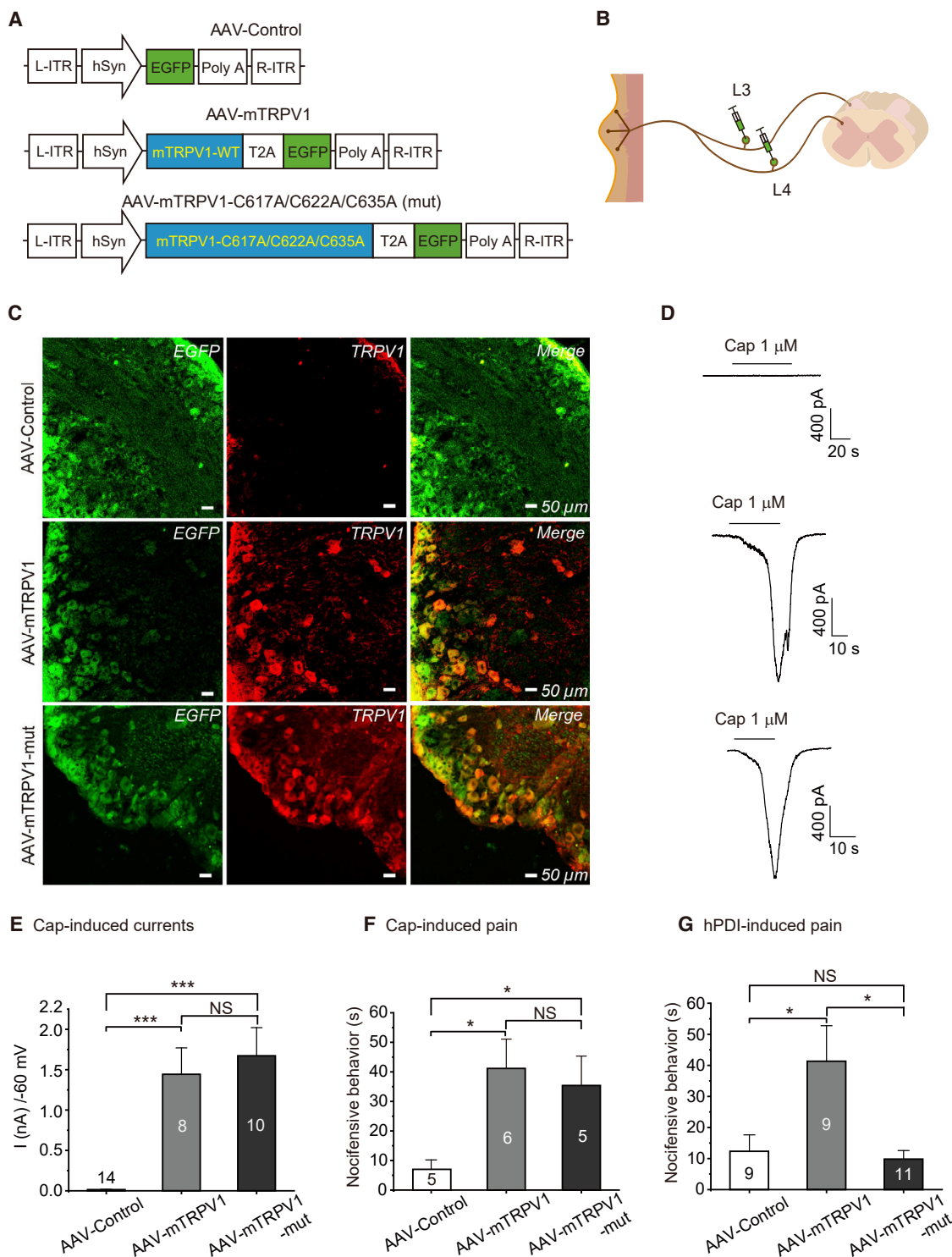
Figure 6. The extracellular cysteines of TRPV1 are critical for hPDI-induced nocifensive behaviors

(A) Diagram depicts the design of AAV-Control, AAV-mTRPV1, and AAV-mTRPV1-mut.

(B) Diagram depicts the sites (L3-L4 DRG) for the injections of designed viruses in TRPV1-KO mice.

(C) Confirmation of viral infection and expression of mTRPV1 and mTRPV1-mut in DRG neurons. Scale bars, 50 μm.

(D and E) Capsaicin elicited comparable inward currents in the DRG neurons from the AAV-mTRPV1 and the AAV-mTRPV1-mut transfected mice, but not from the AAV-Control transfected mice (Kruskal-Wallis H test followed by Nemenyi test, ***$p < 0.001$).

(legend continued on next page)

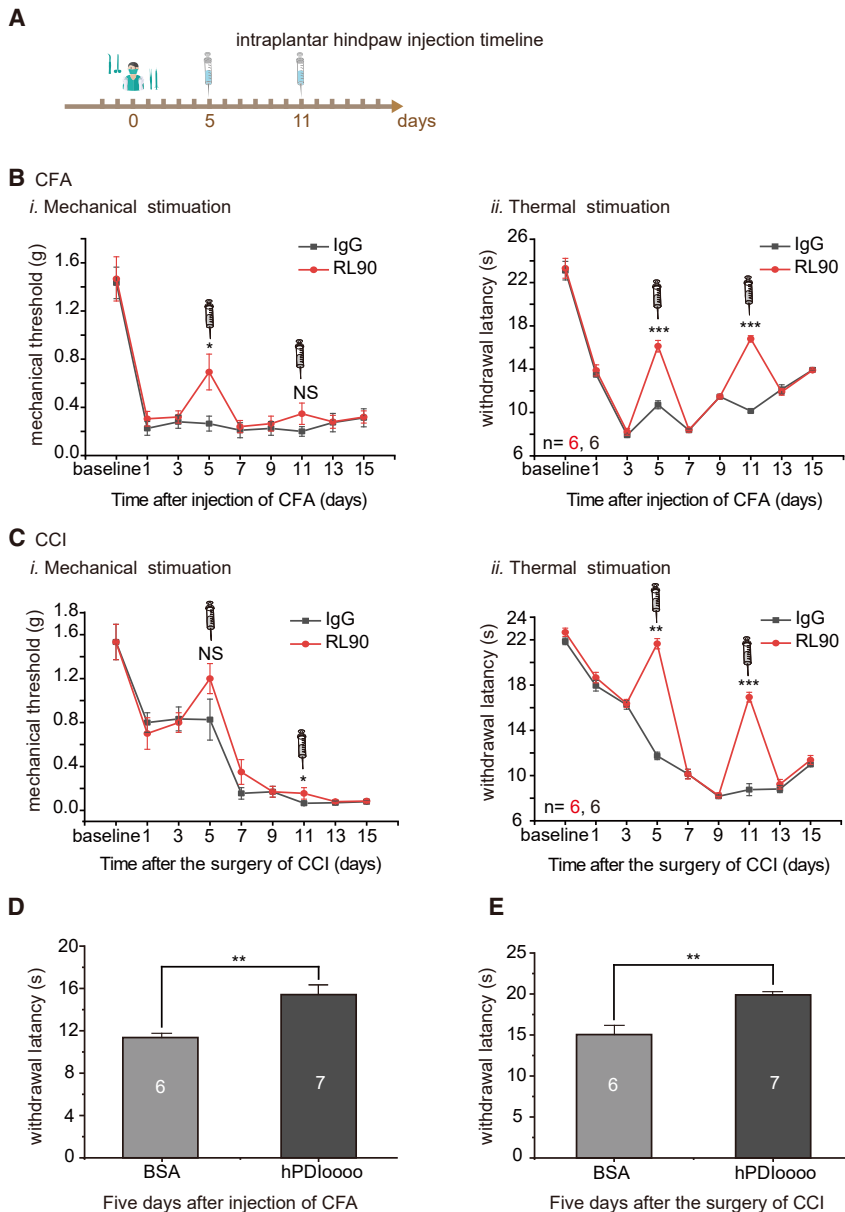**Figure 7. Neutralizing or competitively antagonizing PDI alleviates chronic inflammatory and neuropathic pain**

(A) Mechanical withdrawal threshold and heat withdrawal latency of the mice were tested daily for 16 days, before (day 0) and after intraplantar CFA injection or CCI operation. On the fifth and 11th days after CFA injection or CCI operation, anti-PDI antibody RL90 or IgG was pre-injected 5 h before the nocifensive behavior tests.

(B and C) Thresholds to mechanical stimulus (i) and withdrawal latencies to radiant heat stimulus (ii) are shown for both RL90-and IgG-injected mice of the CFA (B) and CCI (C) model.

(D and E) Pre-injection of inactive hPDIoooo significantly increased heat withdrawal latency in CFA (D) and CCI (E) models. BSA was injected as a control. Two-sample t test, Student's t test or Mann-Whitney U test was used for comparison between groups, *p < 0.05, **p < 0.01, ***p < 0.001. Numbers in bar graphs represent experimental repetitions. Data are represented as mean ± SEM.

in the Nav1.8 (SNS)-expressing nociceptive DRG neurons (Agarwal et al., 2004) blunted the heat hyperalgesia in pathological pain conditions but did not affect the physiological nocifensive behaviors, suggests that the increased activity of PDI was a key element to the heat hyperalgesia specifically and without much contribution to acute physiological pain responses. This distinct modulation of pathological versus physiological heat nocifensive behaviors is almost certainly due to the increased secretion and expression of PDI under pathological pain conditions. Although PDI has a C-terminal ER retention sequence KDEL (Furie and Flaumenhaft, 2014; Hatahet and Ruddock, 2009), PDI secretion has been described in several cell types (albeit not in neurons) (Hahm et al., 2013; Lahav et al., 2002; Mineiro et al., 2020; Swiatkowska et al., 2008). We demonstrate here that PDI could be secreted to both extracellular medium and onto the cell surface of DRG neurons. Chronic inflammation increased the secretion to the extracellular space by ~10% while PDI detectable on the cell surface was increased by ~30%. We believe that both types of secretion could contribute to TRPV1 potentiation by PDI. Here we cannot exclude the possibility that other cells, such as satellite glia, could also secrete PDI in some conditions. Indeed, our immunohistochemical

DISCUSSION

Although a previous proteomic study has reported an upregulated PDI (among other proteins) in DRG neurons in a CFA-induced inflammatory pain model (Rouwette et al., 2016), our study provides a conceptual framework for the role of PDI as a key determinant of heat hyperalgesia in both inflammatory and neuropathic pain. The fact that selective deletion of PDI

(F) Capsaicin elicited comparable nocifensive behaviors in the AAV-mTRPV1 and the AAV-mTRPV1-mut transfected mice, but not the AAV-Control transfected mice (one-way ANOVA with Student-Newman-Keuls post hoc test, *p < 0.05).

(G) hPDI elicited significant nocifensive behavior only in the AAV-mTRPV1 transfected but not in the AAV-mTRPV1-mut transfected mice (Kruskal-Wallis H test followed by Nemenyi test, *p < 0.05). Numbers in bar graphs represent experimental repetitions. Data are represented as mean ± SEM.

analysis shows that PDI is expressed in the satellite glial cells in DRG (data not shown). However, genetic deletion of PDI in Nav1.8-positive neurons specifically, completely abolished the CFA-induced increase of PDI secretion; hence, it is logical to assume that the main source of PDI in chronic inflammation is the DRG neurons.

We provided sufficient evidence to show that PDI induced heat hyperalgesia by activating TRPV1, possibly through an autocrine or paracrine mechanism. TRPV1 in sensory neurons is viewed as an integrator of chemical and physical noxious stimuli (Caterina, 2014; Vay et al., 2012). The channel is activated by capsaicin, temperature (>42°C), protons, and some endogenous molecules (such as certain endocannabinoids) (Hernandez-Araiza et al., 2018; Hwang et al., 2000; Morales-Lazaro et al., 2013, 2017). These agonists activate TRPV1 channels differently (Cao et al., 2013; Gao et al., 2016; Jordt et al., 2000; Yang et al., 2018; Yuan, 2019; Zhang et al., 2021). Lines of evidence have revealed that TRPV1 channels are subject to redox modification (Ogawa et al., 2016; Susankova et al., 2006; Vyklicky et al., 2002). In TRPV1 redox sensing, cysteine modification is considered the principal mechanism. It has been reported that the reducing agent dithiothreitol (DTT) facilitates rat TRPV1 currents induced by capsaicin and heat, to which extracellular cysteine residues C616, C621, and C634 of TRPV1 are believed to be involved (Vyklicky et al., 2002); however, DTT alone did not produce measurable TRPV1 currents. All the above results indicate the complex nature of redox modification of proteins, including TRPV1 cysteines. Unfortunately, the extracellular cysteine-containing region in the resolved rTRPV1 structure is missing because of its dynamic nature (Cao et al., 2013; Gao et al., 2016). A recently resolved full-length squirrel TRPV1 structure (sqTRPV1) by Nadezhdin et al. (2021), revealed the cysteine-containing region assembles into an extracellular cap domain that is important in regulating ion conductance. Our experiments using different plasma-membrane-impermeable oxidative and reducing agents and molecular docking results suggest that the TRPV1 channel should be readily modifiable by oxidated PDI. Our main hypothesis is that PDI physically interacts with TRPV1 and either 1) modulates its activity by facilitating disulfide bond crosslinking within extracellular cysteines of the TRPV1 channel in a "classic" PDI enzyme-catalyzed reaction, or 2) forms a binding complex with TRPV1 by forming disulfide bonds between cysteines in the active center of PDI and extracellular cysteines of TRPV1. In the second case, the activation mechanism could share some similarity with the action of spider toxin, DkTx, which activates TRPV1 by binding to its outer pore region (Cao et al., 2013; Zhang et al., 2021). However, the fact that the catalytically disabled PDI mutant lost its ability to activate TRPV1 and that action of WT PDI is reversed by a reducing agent, TCEP, does suggest that cysteine oxidation is a key to the PDI effect. Future structural studies will be required to elucidate the exact molecular mechanism of this effect. Notably, the TRPV1 channel also contains multiple intracellular cysteine residues, some of which are also reported to be reactive to oxidation (Ogawa et al., 2016). However, our current study focused on the function of secreted PDI acting on the extracellular surface of the plasma membrane.

It is noteworthy that our data show that PDI-induced current is only partially inhibited by a TRPV1 antagonist, which may imply that some other ion channels expressed in DRG neurons could be modulated by PDI. For example, TRPA1 is also reported to be sensitive to redox environmental stimuli (Ibarra and Blair, 2013; Sakaguchi and Mori, 2020; Zhao et al., 2020). We assume TRPV1 may not be the only substrate for PDI modulation in DRG where multiple TRP channels are present. Further experiments are needed to clarify this. However, the experiments with TRPV1-KO mice indicated that TRPV1 is a major contributor to PDI-mediated heat hyperalgesia.

Limitations of study

In the current study, we reported that PDI secreted from primary sensory neurons activates the TRPV1 channel and may be relevant to heat hyperalgesia in pathological pain. We demonstrated that secreted PDI activates the TRPV1 channel by oxidative modulation of extracellular cysteines of TRPV1. However, the exact molecular interactions between two proteins and conformational changes within TRPV1 induced by PDI remain to be elucidated. We believe that future structural studies will shed light on this intriguing question.

STAR★METHODS

Detailed methods are provided in the online version of this paper and include the following:

- KEY RESOURCES TABLE
- RESOURCE AVAILABILITY
  - Lead contact
  - Materials availability
  - Data and code availability
- EXPERIMENTAL MODEL AND SUBJECT DETAILS
  - Experimental animals
  - Human tissue
  - Cells
- METHOD DETAILS
  - Mouse genotyping
  - Immunohistochemistry (IHC)
  - Human tissue and treatment
  - cDNA constructs and mutagenesis
  - Preparation of recombinant human PDI
  - Chronic pain models
  - Behavioral tests
  - ELISA assay
  - Preparation of DRG neuron
  - Flow cytometry experiment
  - HEK 293 cell culture and transfection
  - Electrophysiology
  - Immunoprecipitation and western blot
  - *In vivo* overexpression of mTRPV1 and mTRPV1 mutant
  - Molecular docking and interaction analysis
- QUANTIFICATION AND STATISTICAL ANALYSIS

SUPPLEMENTAL INFORMATION

Supplemental information can be found online at https://doi.org/10.1016/j.celrep.2022.110625.

REFERENCES

Agarwal, N., Offermanns, S., and Kuner, R. (2004). Conditional gene deletion in primary nociceptive neurons of trigeminal ganglia and dorsal root ganglia. Genesis 38, 122–129.

Araujo, T.L.S., Zeidler, J.D., Oliveira, P.V.S., Dias, M.H., Armelin, H.A., and Laurindo, F.R.M. (2017). Protein disulfide isomerase externalization in endothelial cells follows classical and unconventional routes. Free Radic. Biol. Med. 103, 199–208.

Basbaum, A.I., Bautista, D.M., Scherrer, G., and Julius, D. (2009). Cellular and molecular mechanisms of pain. Cell 139, 267–284.

Basso, L., and Altier, C. (2017). Transient receptor potential channels in neuropathic pain. Curr. Opin. Pharmacol. 32, 9–15.

Cao, E., Liao, M., Cheng, Y., and Julius, D. (2013). TRPV1 structures in distinct conformations reveal activation mechanisms. Nature 504, 113–118.

Caterina, M.J. (2014). TRP channel cannabinoid receptors in skin sensation, homeostasis, and inflammation. ACS Chem. Neurosci. 5, 1107–1116.

Chuang, H.H., and Lin, S. (2009). Oxidative challenges sensitize the capsaicin receptor by covalent cysteine modification. Proc. Natl. Acad. Sci. U S A 106, 20097–20102.

Colla, E., Coune, P., Liu, Y., Pletnikova, O., Troncoso, J.C., Iwatsubo, T., Schneider, B.L., and Lee, M.K. (2012). Endoplasmic reticulum stress is important for the manifestations of alpha-synucleinopathy in vivo. J. Neurosci. 32, 3306–3320.

de A Paes, A.M., Verissimo-Filho, S., Guimaraes, L.L., Silva, A.C., Takiuti, J.T., Santos, C.X., Janiszewski, M., Laurindo, F.R., and Lopes, L.R. (2011). Protein disulfide isomerase redox-dependent association with p47(phox): evidence for an organizer role in leukocyte NADPH oxidase activation. J. Leukoc. Biol. 90, 799–810.

Du, X., Hao, H., Gigout, S., Huang, D., Yang, Y., Li, L., Wang, C., Sundt, D., Jaffe, D.B., Zhang, H., et al. (2014). Control of somatic membrane potential in nociceptive neurons and its implications for peripheral nociceptive transmission. Pain 155, 2306–2322.

Du, X., Hao, H., Yang, Y., Huang, S., Wang, C., Gigout, S., Ramli, R., Li, X., Jaworska, E., Edwards, I., et al. (2017). Local GABAergic signaling within sensory ganglia controls peripheral nociceptive transmission. J. Clin. Invest. 127, 1741–1756.

Ellis, R.J. (2013). Assembly chaperones: a perspective. Philos. Trans. R. Soc. Lond. B Biol. Sci. 368, 20110398.

Furie, B., and Flaumenhaft, R. (2014). Thiol isomerases in thrombus formation. Circ. Res. 114, 1162–1173.

Gao, Y., Cao, E., Julius, D., and Cheng, Y. (2016). TRPV1 structures in nanodiscs reveal mechanisms of ligand and lipid action. Nature 534, 347–351.

Goldberger, R.F., Epstein, C.J., and Anfinsen, C.B. (1963). Acceleration of reactivation of reduced bovine pancreatic ribonuclease by a microsomal system from rat liver. J. Biol. Chem. 238, 628–635.

Grand, T., Abi Gerges, S., David, M., Diana, M.A., and Paoletti, P. (2018). Unmasking GluN1/GluN3A excitatory glycine NMDA receptors. Nat. Commun. 9, 4769.

Hahm, E., Li, J., Kim, K., Huh, S., Rogelj, S., and Cho, J. (2013). Extracellular protein disulfide isomerase regulates ligand-binding activity of alphaMbeta2 integrin and neutrophil recruitment during vascular inflammation. Blood 121, 3789–3800.

Hatahet, F., and Ruddock, L.W. (2009). Protein disulfide isomerase: a critical evaluation of its function in disulfide bond formation. Antioxid. Redox Signal. 11, 2807–2850.

Hernandez-Araiza, I., Morales-Lazaro, S.L., Canul-Sanchez, J.A., Islas, L.D., and Rosenbaum, T. (2018). Role of lysophosphatidic acid in ion channel function and disease. J. Neurophysiol. 120, 1198–1211.

Hillson, D.A., Lambert, N., and Freedman, R.B. (1984). Formation and isomerization of disulfide bonds in proteins: protein disulfide-isomerase. Methods Enzymol. 107, 281–294.

Hoffstrom, B.G., Kaplan, A., Letso, R., Schmid, R.S., Turmel, G.J., Lo, D.C., and Stockwell, B.R. (2010). Inhibitors of protein disulfide isomerase suppress apoptosis induced by misfolded proteins. Nat. Chem. Biol. 6, 900–906.

Honjo, Y., Ayaki, T., Tomiyama, T., Horibe, T., Ito, H., Mori, H., Takahashi, R., and Kawakami, K. (2017). Decreased levels of PDI and P5 in oligodendrocytes in Alzheimer's disease. Neuropathology 37, 495–501.

Hwang, S.W., Cho, H., Kwak, J., Lee, S.Y., Kang, C.J., Jung, J., Cho, S., Min, K.H., Suh, Y.G., Kim, D., et al. (2000). Direct activation of capsaicin receptors by products of lipoxygenases: endogenous capsaicin-like substances. Proc. Natl. Acad. Sci. U S A 97, 6155–6160.

Ibarra, Y., and Blair, N.T. (2013). Benzoquinone reveals a cysteine-dependent desensitization mechanism of TRPA1. Mol. Pharmacol. 83, 1120–1132.

Jordt, S.E., Tominaga, M., and Julius, D. (2000). Acid potentiation of the capsaicin receptor determined by a key extracellular site. Proc. Natl. Acad. Sci. U S A 97, 8134–8139.

Kim, J.Y., Ko, A.R., Hyun, H.W., Min, S.J., and Kim, J.E. (2017). PDI regulates seizure activity via NMDA receptor redox in rats. Sci. Rep. 7, 42491.

Lahav, J., Jurk, K., Hess, O., Barnes, M.J., Farndale, R.W., Luboshitz, J., and Kehrel, B.E. (2002). Sustained integrin ligation involves extracellular free sulfhydryls and enzymatically catalyzed disulfide exchange. Blood 100, 2472–2478.

Li, X., Zhang, B., Yan, C., Li, J., Wang, S., Wei, X., Jiang, X., Zhou, P., and Fang, J. (2019). A fast and specific fluorescent probe for thioredoxin reductase that works via disulphide bond cleavage. Nat. Commun. 10, 2745.

Lyles, M.M., and Gilbert, H.F. (1991). Catalysis of the oxidative folding of ribonuclease A by protein disulfide isomerase: dependence of the rate on the composition of the redox buffer. Biochemistry 30, 613–619.

Massignan, T., Casoni, F., Basso, M., Stefanazzi, P., Biasini, E., Tortarolo, M., Salmona, M., Gianazza, E., Bendotti, C., and Bonetto, V. (2007). Proteomic analysis of spinal cord of presymptomatic amyotrophic lateral sclerosis G93A SOD1 mouse. Biochem. Biophys. Res. Commun. 353, 719–725.

Matsusaki, M., Kanemura, S., Kinoshita, M., Lee, Y.H., Inaba, K., and Okumura, M. (2020). The protein disulfide isomerase family: from proteostasis to pathogenesis. Biochim. Biophys. Acta Gen. Subj. *1864*, 129338.

Mineiro, M.F., Patricio, E.S., Peixoto, A.S., Araujo, T.L.S., da Silva, R.P., Moretti, A.I.S., Lima, F.S., Laurindo, F.R.M., and Meotti, F.C. (2020). Urate hydroperoxide oxidizes endothelial cell surface protein disulfide isomerase-A1 and impairs adherence. Biochim. Biophys. Acta Gen. Subj. *1864*, 129481.

Morales-Lazaro, S.L., Lemus, L., and Rosenbaum, T. (2017). Regulation of thermoTRPs by lipids. Temperature (Austin) *4*, 24–40.

Morales-Lazaro, S.L., Simon, S.A., and Rosenbaum, T. (2013). The role of endogenous molecules in modulating pain through transient receptor potential vanilloid 1 (TRPV1). J. Physiol. *591*, 3109–3121.

Moran, M.M., and Szallasi, A. (2018). Targeting nociceptive transient receptor potential channels to treat chronic pain: current state of the field. Br. J. Pharmacol. *175*, 2185–2203.

Nadezhdin, K.D., Neuberger, A., Nikolaev, Y.A., Murphy, L.A., Gracheva, E.O., Bagriantsev, S.N., and Sobolevsky, A.I. (2021). Extracellular cap domain is an essential component of the TRPV1 gating mechanism. Nat. Commun. *12*, 2154.

Ogawa, N., Kurokawa, T., Fujiwara, K., Polat, O.K., Badr, H., Takahashi, N., and Mori, Y. (2016). Functional and structural divergence in human TRPV1 channel subunits by oxidative cysteine modification. J. Biol. Chem. *291*, 4197–4210.

Okumura, M., Noi, K., Kanemura, S., Kinoshita, M., Saio, T., Inoue, Y., Hikima, T., Akiyama, S., Ogura, T., and Inaba, K. (2019). Dynamic assembly of protein disulfide isomerase in catalysis of oxidative folding. Nat. Chem. Biol. *15*, 499–509.

Pan, B., Akyuz, N., Liu, X.P., Asai, Y., Nist-Lund, C., Kurima, K., Derfler, B.H., Gyorgy, B., Limapichat, W., Walujkar, S., et al. (2018). TMC1 forms the pore of mechanosensory transduction channels in vertebrate inner ear hair cells. Neuron *99*, 736–753.e36.

Perri, E., Parakh, S., and Atkin, J. (2017). Protein disulphide isomerases: emerging roles of PDI and ERp57 in the nervous system and as therapeutic targets for ALS. Expert Opin. Ther. Targets *21*, 37–49.

Pirneskoski, A., Klappa, P., Lobell, M., Williamson, R.A., Byrne, L., Alanen, H.I., Salo, K.E., Kivirikko, K.I., Freedman, R.B., and Ruddock, L.W. (2004). Molecular characterization of the principal substrate binding site of the ubiquitous folding catalyst protein disulfide isomerase. J. Biol. Chem. *279*, 10374–10381.

Reinhardt, C., von Bruhl, M.L., Manukyan, D., Grahl, L., Lorenz, M., Altmann, B., Dlugai, S., Hess, S., Konrad, I., Orschiedt, L., et al. (2008). Protein disulfide isomerase acts as an injury response signal that enhances fibrin generation via tissue factor activation. J. Clin. Invest. *118*, 1110–1122.

Rouwette, T., Sondermann, J., Avenali, L., Gomez-Varela, D., and Schmidt, M. (2016). Standardized profiling of the membrane-enriched proteome of mouse dorsal root ganglia (DRG) provides novel insights into chronic pain. Mol. Cell Proteomics *15*, 2152–2168.

Sakaguchi, R., and Mori, Y. (2020). Transient receptor potential (TRP) channels: biosensors for redox environmental stimuli and cellular status. Free Radic. Biol. Med. *146*, 36–44.

Susankova, K., Tousova, K., Vyklicky, L., Teisinger, J., and Vlachova, V. (2006). Reducing and oxidizing agents sensitize heat-activated vanilloid receptor (TRPV1) current. Mol. Pharmacol. *70*, 383–394.

Swiatkowska, M., Szymanski, J., Padula, G., and Cierniewski, C.S. (2008). Interaction and functional association of protein disulfide isomerase with alphaVbeta3 integrin on endothelial cells. FEBS J. *275*, 1813–1823.

Tominaga, M., Caterina, M.J., Malmberg, A.B., Rosen, T.A., Gilbert, H., Skinner, K., Raumann, B.E., Basbaum, A.I., and Julius, D. (1998). The cloned capsaicin receptor integrates multiple pain-producing stimuli. Neuron *21*, 531–543.

Vay, L., Gu, C., and McNaughton, P.A. (2012). The thermo-TRP ion channel family: properties and therapeutic implications. Br. J. Pharmacol. *165*, 787–801.

Venetianer, P., and Straub, F.B. (1963). The enzymic reactivation of reduced ribonuclease. Biochim. Biophys. Acta *67*, 166–168.

Vyklicky, L., Lyfenko, A., Susankova, K., Teisinger, J., and Vlachova, V. (2002). Reducing agent dithiothreitol facilitates activity of the capsaicin receptor VR-1. Neuroscience *111*, 435–441.

Wang, C., Li, W., Ren, J., Fang, J., Ke, H., Gong, W., Feng, W., and Wang, C.C. (2013). Structural insights into the redox-regulated dynamic conformations of human protein disulfide isomerase. Antioxid. Redox Signal. *19*, 36–45.

Wei, N.N., Lv, H.N., Wu, Y., Yang, S.L., Sun, X.Y., Lai, R., Jiang, Y., and Wang, K. (2016). Selective activation of nociceptor TRPV1 channel and reversal of inflammatory pain in mice by a novel coumarin derivative muralatin L from murraya alata. J. Biol. Chem. *291*, 640–651.

Wilkinson, B., and Gilbert, H.F. (2004). Protein disulfide isomerase. Biochim. Biophys. Acta *1699*, 35–44.

Yang, F., Cui, Y., Wang, K., and Zheng, J. (2010). Thermosensitive TRP channel pore turret is part of the temperature activation pathway. Proc. Natl. Acad. Sci. U S A *107*, 7083–7088.

Yang, F., Xiao, X., Lee, B.H., Vu, S., Yang, W., Yarov-Yarovoy, V., and Zheng, J. (2018). The conformational wave in capsaicin activation of transient receptor potential vanilloid 1 ion channel. Nat. Commun. *9*, 2879.

Yang, L., Dong, F., Yang, Q., Yang, P.F., Wu, R., Wu, Q.F., Wu, D., Li, C.L., Zhong, Y.Q., Lu, Y.J., et al. (2017). FGF13 selectively regulates heat nociception by interacting with Nav1.7. Neuron *93*, 806–821.e9.

Yuan, P. (2019). Structural biology of thermoTRPV channels. Cell Calcium *84*, 102106.

Zhang, K., Julius, D., and Cheng, Y. (2021). Structural snapshots of TRPV1 reveal mechanism of polymodal functionality. Cell *184*, 5138–5150.e12.

Zhao, J., Lin King, J.V., Paulsen, C.E., Cheng, Y., and Julius, D. (2020). Irritant-evoked activation and calcium modulation of the TRPA1 receptor. Nature *585*, 141–145.

Zhou, J., Wu, Y., Wang, L., Rauova, L., Hayes, V.M., Poncz, M., and Essex, D.W. (2015). The C-terminal CGHC motif of protein disulfide isomerase supports thrombosis. J. Clin. Invest. *125*, 4391–4406.

STAR★METHODS

KEY RESOURCES TABLE

REAGENT or RESOURCE	SOURCE	IDENTIFIER
Antibodies		
Mouse monoclonal anti-NF200	Sigma-Aldrich	Cat#N0142; RRID: AB_477257
Mouse monoclonal anti-CGRP (4901)	Santa Cruz	Cat#sc-57053; RRID: AB_2259462
Mouse monoclonal anti-CGRP (4901)	Abcam	Cat#ab81887; RRID: AB_1658411
IB4	Sigma-Aldrich	Cat#L2895; RRID: N/A
Rabbit polyclonal anti-PDI (H-160)	Santa Cruz	Cat#sc-20132; RRID: AB_653974
Rabbit monoclonal anti-PDI (C81H6)	Cell Signaling Technology	Cat#3501; RRID: AB_2156433
PE Rabbit monoclonal anti-P4HB (EPR9499)	Abcam	Cat#ab210594; RRID: N/A
PE Rabbit monoclonal anti-IgG (EPR25A)	Abcam	Cat#ab209478; RRID: N/A
Mouse monoclonal anti-VR1 (E-8)	Santa Cruz	Cat#sc-398417; RRID: AB_2827686
Mouse monoclonal anti-TRPV1 (BS397) C-terminal	Abcam	Cat#ab203103; RRID: N/A
Mouse monoclonal anti-PDI (C-2)	Santa Cruz	Cat#sc-74551; RRID: AB_2156462
Rabbit polyclonal anti-PDI	Enzo Life Sciences	Cat#ADI-SPA-890-F; RRID: N/A
Rabbit polyclonal anti-GFP	Abcam	Cat#ab290; RRID: AB_303395
Mouse monoclonal anti-His	GenScript	Cat#A00186; RRID: AB_914704
Mouse monoclonal anti-P4HB (RL90)	Abcam	Cat#ab2792; RRID: AB_303304
Mouse monoclonal anti-Tubulin β 3	Biolegend	Cat#801201; RRID: AB_2313773
Rabbit polyclonal anti- GFAP	Servicebio	Cat#GB11096; RRID: AB_2904015
Bacterial and virus strains		
AAV9-Control	Genechem	N/A
AAV9-mTRPV1-T2A-EGFP	Genechem	N/A
AAV9-mTRPV1(C617A/C622A/C635A)-T2A-EGFP	Genechem	N/A
AAV9-CAG-EGFP	Genechem	N/A
AAV9-CAG-EGFP-T2A-Cre	Genechem	N/A
Biological samples		
Postmortem human DRGs	The Forth Hospital of Shijiazhuang	N/A
Chemicals, peptides, and recombinant proteins		
Freund's Adjuvant, Complete (CFA)	Sigma-Aldrich	Cat#F5881
Capsaicin	Sigma-Aldrich	Cat#360376
Capsazepine	GlpBio	Cat#GC17918
Sodium (2-Sulfonatoethyl) methanethiol sulfonate (MTSES)	Toronto Research Chemicals	Cat#S672000
5, 5-dithio-bis (2-nitrobenzoic acid) [DTNB]	Solarbio	Cat#D8350
L-Glutathione reduced (L-GSH)	Sigma-Aldrich	Cat#G4251
Tris(2-carboxyethyl) phosphine hydrochloride (TCEP·HCl)	Sigma-Aldrich	Cat#C4706
Dithiothreitol (DTT)	Sigma-Aldrich	Cat#V900830
recombinant proteins hPDI	GenScript Biotechnology	N/A
recombinant proteins hPDIoooo (C53S, C56S and C397S, C400S)	GenScript Biotechnology	N/A
Critical commercial assays		
PDI ELISA development set	Enzo Life Sciences	Cat#ADI-960-072
Experimental models: Cell lines		
HEK293 cells	Kunming Cell Bank	Cat#KCB2000408YJ
Experimental models: Organisms/strains		
Pdi-floxed mice (C57BL/6J & 129Sv)	Zhou, et al., 2015	N/A
SNS-Cre mice (C57BL/6)	Yang, et al., 2017	N/A
TRPV1-KO mice (B6.129X1-Trpv1^tm1Jul/J)	The Jackson Laboratory	Cat#003770

Continued

REAGENT or RESOURCE	SOURCE	IDENTIFIER
Oligonucleotides		
Cre-F: 5′-ATTTGCCTGCATTACCGGTC-3′	SBS Genetech	N/A
Cre-R: 5′-GCATCACGTTTTCTTTTCGG-3′	SBS Genetech	N/A
PDI-F: 5′-TCTGGAAAAGGAAGTCCAACCGAGA-3′	SBS Genetech	N/A
PDI-R: 5′-AAGTCTCCTCAAGGAAGCCAGGGAC-3′	SBS Genetech	N/A
TRPV1-KO PRIMER1: 5′-TGGCTCATATTTGCCTTCAG-3′	SBS Genetech	N/A
TRPV1-KO PRIMER2: 5′-CAGCCCTAGGAGTTGATGGA-3′	SBS Genetech	N/A
TRPV1-KO PRIMER3: 5′-TAAAGCGCATGCTCCAGACT-3′	SBS Genetech	N/A
Recombinant DNA		
His-hPDI	Zhou, et al., 2015	N/A
His-hPDIoooo	Zhou, et al., 2015	N/A
mTRPV1-GFP	This paper	N/A
mTRPV1-GFP mutation (C617A/C622A/C635A)	Takara Biomedical Technology	N/A
hTRPV1-IRSE2-EGFP	Wei, et al., 2016	N/A
hTRPV1-IRSE2-EGFP mutation (C621A/C635A)	Takara Biomedical Technology	N/A
Software and algorithms		
IBM SPSS Statistics 21.0	IBM Corporation	https://www.ibm.com/products/spss-statistics
OriginPro 2018	OriginLab Corporation	https://www.originlab.com/
Clampfit 10.3	Molecular Devices	https://www.moleculardevices.com/

RESOURCE AVAILABILITY

Lead contact
Further information and requests for resources and reagents should be directed to and will be fulfilled by the Lead Contact, Xiaona Du (duxiaona@hebmu.edu.cn).

Materials availability
This study did not generate new unique reagents.

Data and code availability
- All data reported in this paper will be shared by the Lead contact upon reasonable request.
- This paper does not report original code.
- Any additional information required to reanalyze the data reported in this paper is available from the Lead contact upon reasonable request.

EXPERIMENTAL MODEL AND SUBJECT DETAILS

Experimental animals
PDI-floxed mice (C57BL/6J & 129Sv) were provided by professor Yi Wu (Soochow University, Suzhou, China (Zhou et al., 2015)), and SNS-Cre mice (C57BL/6) were provided by professor Xu Zhang (Chinese Academy of Sciences, Shanghai, China (Yang et al., 2017)). SNS-Cre,PDI$^{fl/fl}$ mice and the littermate control were generated by mating SNS-Cre mice with PDI-floxed mice. TRPV1-KO mice (B6.129X1-Trpv1^{tm1Jul}/J) were provided by Professor Shilong Yang (Chinese Academy of Sciences, Yunnan, China). Adult male C57BL/6 mice (6–8 weeks) were bought from Vital River (Beijing, China). Mice were housed at constant temperature and humidity, under a 12 h: 12 h light-dark cycle (switches at 8 AM and 8 PM), with *ad libitum* access to water and food. All animal experiments were approved by the Animal Care and Ethical Committee of Hebei Medical University (The ethical approval reference number: IACUC-Hebmu-2020007) and were in accordance with the International Association for the Study of Pain guidelines for animal use.

Human tissue
Human embryonic DRGs were obtained from the Forth Hospital of Shijiazhuang. The study protocols concerning human tissues are consistent with the principles of the Declaration of Helsinki and were approved by the Clinical Research Ethics Committee of Hebei Medical University and the Forth Hospital of Shijiazhuang.

Cells

HEK293 cells were purchased from Kunming Cell Bank (Cat#: KCB2000408YJ) and cultured at 37°C in 5% CO_2 incubator using DMEM culturing media containing 10% BSA, 1% penicillin and streptomycin mixture.

METHOD DETAILS

Mouse genotyping

Mouse genomic DNA was extracted from 0.5 cm clipped tail specimen, which lysed in 100 μL NaOH (50 mM), 95°C for 30 min and neutralized with 30 μL Tris-HCl (1 M, pH = 7.2). Genotyping was performed by PCR with 35 cycles of 95°C for 1 min, 55°C for 50 s, and 72°C for 1 min. The primers for SNS-Cre were 5′-ATTTGCCTGCATTACCGGTC-3′ and 5′-GCATCACGTTTTCTTTTCGG-3′, and the expected product size was about 300 bp. The primers for PDI-floxed were 5′-TCTGGAAAAGGAAGTCCAACCGAGA-3′ and 5′-AAGTCTCCTCAAGGAAGCCAGGGAC-3′, and the product sizes were 400–500 bp (WT) and 500–600 bp (*loxP*). The primers for TRPV1-KO were 5′-TGGCTCATATTTGCCTTCAG-3′, 5′-CAGCCCTAGGAGTTGATGGA-3′ and 5′-TAAAGCGCATGCTCCAGACT-3′, and the product sizes were about 289 bp (WT) and 176 bp (KO). The primers were synthesized by SBS Genetech Co., Ltd (Beijing, China).

Immunohistochemistry (IHC)

Mouse lumbar DRGs were extracted as described previously (Du et al., 2017) and embedded in Tissue-Tek O.C.T. (Sakura, USA), frozen at −80°C, overnight. 10 μm DRG slices were cut using microtome (Leica, Germany) and fixed in 4% paraformaldehyde (PFA) for 15 min at room temperature. Sections were washed three times with PBS and permeabilized with 0.1% Triton X-100 for 10 min at room temperature. After blocking DRG slices with blocking buffer (PBS containing 10% donkey serum) for 30–60 min at room temperature, the sections were incubated with the primary antibodies at 4°C, overnight. On the second day, the sections were washed three times with PBS and stained with fluorophore-conjugated secondary antibodies for 2 h at room temperature. The sections were then washed with PBS three times and mounted with an enhanced antifade mounting medium (IH0253-0321A18, Leagene, Beijing, China). All images were collected on a Leica inverted confocal microscope (Model: SP5, Wetzlar, Germany) with a 20× or 10× dry objective.

Human tissue and treatment

Paraffin-embedded hDRG tissue sections (2 μm) were deparaffinized in xylene and rehydrated with graded ethanol. Antigen retrieval was subsequently performed by autoclaving for 10 min at 121°C in a sodium citrate buffer (pH 6.0). After rinsing with PBS (pH 7.4). Internal peroxidase was inactivated with 3% hydrogen peroxide in 100% methanol for 20 min at room temperature. Rinsing with PBS again. After blocking with 10% normal goat serum for 30 min at 37°C, the sections were incubated with primary antibodies overnight at 4°C. The next day, sections were washed with PBS. The tissue was then exposed to fluorophore-conjugated secondary antibody for 2 h at 37°C. Immunofluorescence was then examined by laser confocal microscopy.

cDNA constructs and mutagenesis

mTRPV1-GFP plasmid was kindly provided by Professor Hailong An (Hebei University of Technology, Tianjin, China). hTRPV1 was kindly provided by Professor Kewei Wang (Qingdao University, Qingdao, China (Wei et al., 2016)). mTRPV1-GFP mutation (C617A/C622A/C635A) and hTRPV1 mutation (C621A/C635A) were generated by Takara Biomedical Technology Co., Ltd (Beijing, China).

Preparation of recombinant human PDI

The E. coli strain BL21 (DE3) containing cDNA for human PDI (hPDI) in the pTrix-4 Neo vector with an N-terminal histidine tag and the active sites mutation one named hPDIoooo (C53S, C56S and C397S, C400S) were obtained from Professor Yi Wu (Soochow University, Suzhou, China (Zhou et al., 2015)). Recombinant human PDI was generated by GenScript Biotechnology Co., Ltd (Nanjing, China). Briefly, BL21 (DE3) stored in glycerol was inoculated into LB medium containing ampicillin and cultured at 37°C. When the OD600 reached about 1.2, cell culture was induced with IPTG at 37°C for 4 h. Cells were harvested by centrifugation. Cell pellets were resuspended with lysis buffer followed by sonication. The supernatant after centrifugation was kept for future purification. Protein was obtained by two-step purification using Ni column and Superdex 200 column (GE Healthcare, USA). Target protein were dialyzed and sterilized by 0.22 μm filter before being stored in aliquots. The concentration was determined by Bradford protein assay (Thermo Fisher, Shanghai, China) with bovine serum albumin (BSA) as a standard. The protein purity and molecular weight were determined by standard SDS-PAGE. Reductase activity of the hPDI was determined against Di-E-GSSG (Soochow University, Suzhou, China) in PDI assay buffer (0.1 M potassium phosphate buffer, 2 mM EDTA, pH 7.0) by adding PDI (100 nM) to Di-E-GSSG (150 nM) in the presence of 5 μM DTT (Dithiothreitol). The increase in fluorescence was monitored by microplate reader (FLUOstar Omega, BMG LABTECH, Germany) at 545 nm, with excitation at 525 nm.

Chronic pain models

To induce chronic neuropathic pain, mice were anesthetized with an i. p. injection of 0.1 mL 1% sodium pentobarbital. The right hind leg was shaved and cleaned using 75% ethanol. The sciatic nerve was exposed by blunt dissection at the mid-thigh level, proximal to

the sciatic trifurcation. Three nonabsorbable sterile surgical sutures (4–0 chromic gut) were loosely tied around the sciatic nerve with approximately 1.0 mm interval between the knots. The skin was sutured, and the animal was transferred to a recovery cage. To induce chronic inflammatory pain, Complete Freund's adjuvant (CFA, 25 μL) was injected into the plantar surface of the right hind paw of the mice.

Behavioral tests

In all tests, animals were habituated to the testing environment for at least 1 h before behavioral testing. In PDI induced pain test, hPDI (25 μL, 50 μM or 100 μM), hPDIoooo (25 μL, 50 μM) or Saline (25 μL) were injected into the right hind paw. After the injections, animals were returned to the cage and video-recorded for 30 min. Time of licking, biting, and flinching of the injected paw was analyzed by operator blind to the composition of the drug solution. Mechanical and thermal sensitivity were analyzed using von Frey and Hargreaves methods, respectively as previously described (Du et al., 2017). In hot plate test, Mice were placed on a hot plate at a certain temperature of 48°C, 50°C, 52°C, 54°C, 56°C. The response latency was recorded when the mice licking the right hind paw. The cutoff time was 60 s to prevent scalding. In Tail-Flick test, the lower third of the mouse tail was vertically immerged into a water bath at a certain temperature of 46°C, 48°C, 50°C, 52°C. The latency was recorded when the tails withdrawed from the water. The cutoff time was 20 s to prevent scalding.

ELISA assay

DRG tissue were extracted from experimental mice (20–25 g) humanely euthanized by cervical dislocation. Extrated DRG were rapidly transferred into incubation solution on ice and washed once. The incubation solution containing (in mM): 160 NaCl, 2.5 KCl, 5 CaCl$_2$, 1 MgCl$_2$, 10 HEPES, 8 D-glucose, pH = 7.4. The DRG was then incubated in 500 μL solution for 30 min at room temperature. After incubation, the supernatant was collected after centrifugation gently and stored at 4°C. On the following day, ELISA process was operated according to the instructions of PDI ELISA development set (ADI-960-072, Enzo Life Sciences, USA).

Preparation of DRG neuron

DRG neurons were dissociated as described previously (Du et al., 2017). Briefly, adult mice (20–25 g) were humanely euthanized by cervical dislocation. DRG from all spinal levels or L3-L5 levels were removed and treated at 37°C in Hank's Balanced Salt Solution supplemented with collagenase (2.5 mg/mL) and dispase (7.5 mg/mL) for about 30 min. Ganglia were then gently washed twice and resuspended in 3 mL DMEM culturing media containing 10% BSA, 1% penicillin and streptomycin mixture. For patch clamp recording, this suspension was then plated on glass coverslips coated with 0.5 mg/mL poly-D-lysine, and cultured at 37°C in 5% CO$_2$ incubator.

Flow cytometry experiment

Dissociated murine DRG neurons were filtered through nylon sieve, then diluted into 400 μL PBS (cell counts $\geq 1.0 \times 10^6$) and incubated with PE-conjugated PDI antibody (1:1000) or PE-conjugated IgG (1:1000) for 1 h at room temperature in the dark. Samples were analyzed by flow cytometry (ACEABIO, NovoCyte, USA). PBS (phosphate buffered saline) contains 137 NaCl, 2.7 KCl, 10 Na$_2$HPO$_3$, KH$_2$PO$_3$ in mM and pH = 7.4.

HEK 293 cell culture and transfection

HEK293 cells were cultured at 37°C in 5% CO$_2$ incubator using DMEM culturing media containing 10% BSA, 1% penicillin and streptomycin mixture. Cell grown into about 80% confluence were transfected with the desired DNA constructs using transfection reagent following the protocol provided by the instructions.

Electrophysiology

For recordings on DRG neurons, perforated (with 0.4 mg/mL amphotericin, Sigma-Aldrich, USA) patch-clamp recordings in current- or voltage clamp configurations were performed on dissociated DRG neurons with access resistance of 3–5 MΩ typically. Currents were amplified and recorded using an Axon Patch 700B amplifier and pClamp 10.0 software (Axon Instruments, USA), and were sampled at 5 kHz. Liquid junction potentials were calculated using the pClamp and corrected. Continuous current-clamp with no current injection was used for monitoring membrane potential. Linear ramps of currents from 0 to 1 nA (1000 ms or 1200 ms duration) were injected for measuring firing of action potential (AP) firing.

For recordings on HEK293 cells, voltage-clamp recordings were made in the whole cell configuration in gap-free model (holding at −60 mV, sampled at 1 kHz) and ramp stimulation (from −100 mV to +100 mV, duration 800 ms, interval 20 s, sampled at 1 kHz) on HEK293 transfected with the desired plasmid(s) with access resistance 3–5 MΩ.

All recordings were performed at room temperature. The extracellular solution contained (in mM):160 NaCl, 2.5 KCl, 5 CaCl$_2$, 1MgCl$_2$, 10 HEPES, and 8 glucose (pH 7.4). The intracellular solution contained (in mM): 150 KCl, 5 MgCl$_2$, 10 HEPES (pH 7.4).

Immunoprecipitation and western blot

Lumbar DRG were extracted and lysed in IP lysis buffer (Thermo, USA). HEK 293 cells co-transfected with mTRPV1-GFP and His-hPDI were harvested and lysed in IP lysis buffer by sonication. The lysed tissues were centrifuged for 30 min at 12,000 rpm and 4°C,

the supernatant of the lysate was transferred to a new tube. A/G-Sepharose beads (Santa Cruz, USA) were used to purify the supernatant which was incubated with bait protein antibody overnight at $4°C$; or Ni columns (GE Healthcare, USA) were used to purify the supernatant directly. The target proteins were boiled in SDS sample buffer at $95°C$ for 10 min before being subject to SDS-PAGE and immunoblotting. The western blot was carried out according to the standard protocol.

In vivo overexpression of mTRPV1 and mTRPV1 mutant

Overexpression of the mTRPV1 and the mutant channels into TRPV1-null DRG neurons were achieved by affecting the DRG with AAV9 virus carrying the channel DNA sequence, and were produced by Genechem Co., Ltd (Shanghai, China). The mouse TRPV1 DNA sequence was referenced from NCBI (GenBank: NM_001001445). The constructs containing the wild type and mutant channels with EGFP (mTRPV1-T2A-EGFP, and the mutant mTRPV1(C617A/C622A/C635A)-T2A-EGFP) were constructed and amplified using PCR, and were cloned into hSyn-MCS-SV40 vector. AAV9-Control (1.27×10^{13} µg/mL), AAV9-mTRPV1-T2A-EGFP (4.85×10^{12} µg/mL), AAV9-mTRPV1- (C617A/C622A/C635A)-T2A-EGFP (4.27×10^{12} µg/mL) were produced by cotransfecting the desired pAAV plasmid, pHelper and pAAV-RC into AAV-HEK293 cells. 72 h later, viral particles were collected, concentrated and purified. The above-mentioned AAV9 virus were injected into the DRG (right L3–L4) of the TRPV1-knockout (TRPV1-KO) mice. Mice were anaesthetized with 1% pentobarbital sodium and ganglions were exposed surgically. Viral solution was diluted with equal volume PBS and injected into the exposed DRG at a rate of 0.2 µL/min (2 µL per DRG) with a glass micropipette connected to a Hamilton syringe controlled by a microsyringe pump controller (78–8130, KD Scientific, USA). The glass micropipette was removed after 10 min, then the skin was sutured, the animal was transferred to a recovery cage. Mice were used for experiments 4 weeks later.

Molecular docking and interaction analysis

mTRPV1 and hTRPV1 structure used in the molecular simulation was obtained using homology modeling server SWISSMODODEL based on the structure of rTRPV1 (protein databank, PDB: 3j5p). CHARMM-GUI server was used to construct TRPV system with lipid, water, and ion. Molecular dynamics simulation software Amber was used to do energy minimization and dynamic equilibrium of mTRPV1 and hTRPV1 system. Docking server ZDOCK was used to perform molecular docking between constructed mTRPV1 and hTRPV1 (receptor protein) structure and structures of PDI (ligand protein), including oxidized hPDI (PDB: 4el1) or reduced PDI (PDB: 4ekz).

QUANTIFICATION AND STATISTICAL ANALYSIS

All data are given as mean ± SEM. Differences between groups were assessed by Student t-test or t'-test (normal distribution data) or Mann-Whitney U test(data failed normality test). Multiple groups were compared using one-way ANOVA with Student-Newman-Keuls post hoc test (normal distribution data) or Kruskal-Wallis H test with Nemenyi post hoc test (data failed normality test). Hyperalgesia data in chronic pain model was analyzed using repeated measures ANOVA. Differences were considered significant at $p \leq 0.05$. Statistical analyses were performed using IBM SPSS statistics. In bar charts shown in the figures, number of experiments is indicated within or above each bar; single, double, and triple asterisks indicate significant difference with $p \leq 0.05$, 0.01, or 0.001, respectively.

Supplemental information

Protein disulfide isomerase

modulation of TRPV1 controls

heat hyperalgesia in chronic pain

Yongxue Zhang, Qi Miao, Sai Shi, Han Hao, Xinmeng Li, Zeyao Pu, Yakun Yang, Hailong An, Wei Zhang, Youzhen Kong, Xu Pang, Cunyang Gu, Nikita Gamper, Yi Wu, Hailin Zhang, and Xiaona Du
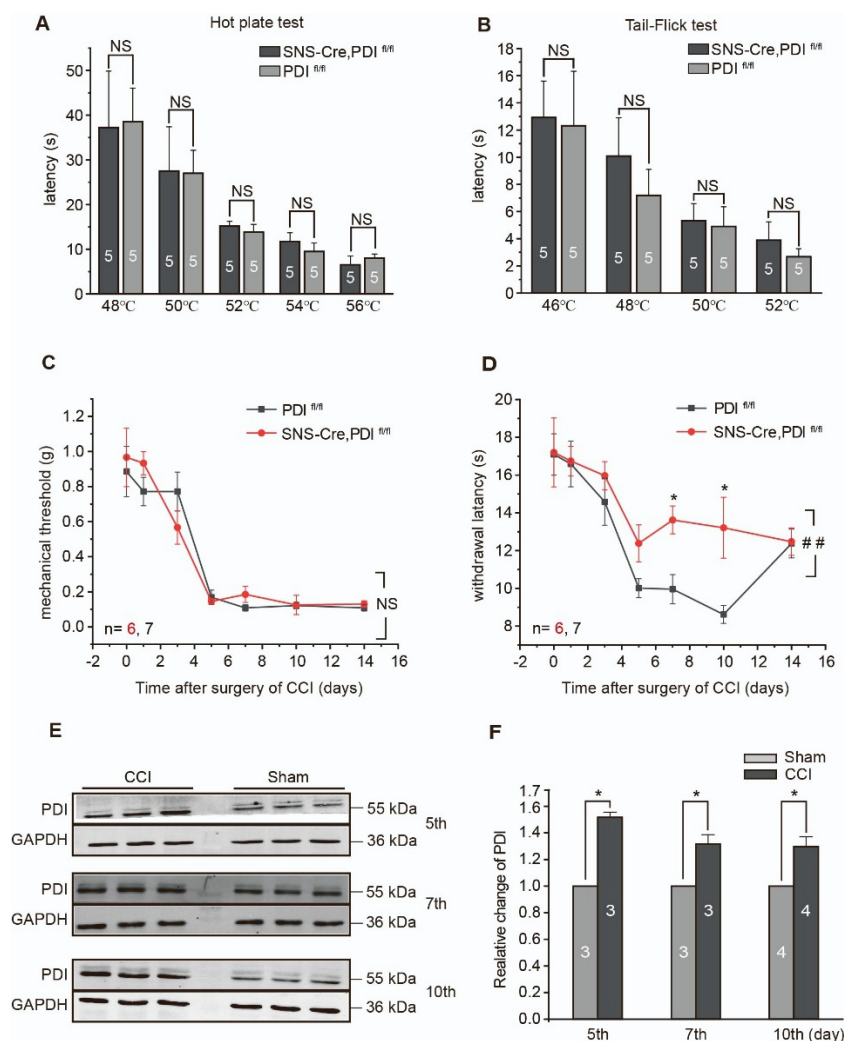
Supplementary materials

Figure S1. PDI protein is important for heat hyperalgesia of neuropathic pain. Related to Figure 1.

(A and B) Withdrawal latencies to a range of temperature stimuli in hot plate test and tail flick test. No differences were observed between the PDI$^{fl/fl}$ mice and the SNS-Cre,PDI$^{fl/fl}$ mice , T test or Mann-Whitney U test, $p > 0.05$.

(C) Mechanical thresholds of SNS-Cre,PDI$^{fl/fl}$ mice and PDI$^{fl/fl}$ mice subjected to CCI surgery. Repeated measures ANOVA, $p > 0.05$.

(D) Withdrawal latencies of SNS-Cre,PDI$^{fl/fl}$ mice and PDI$^{fl/fl}$ mice subjected to CCI surgery. Repeated measures ANOVA, # #$p < 0.01$,student t test or Mann-Whitney U test was used for test difference between two groups within the corresponding time point, *$P < 0.05$, **$P < 0.01$, NS, not significant.

(E) Western blot of PDI protein in the DRG tissue of wild type mice on 5th, 7th and 10th day after CCI operation.

(F) Summary for E (One sample t test, *$p < 0.05$). Numbers in bar graphs represent experimental repetitions. Data are represented as mean ± SEM.
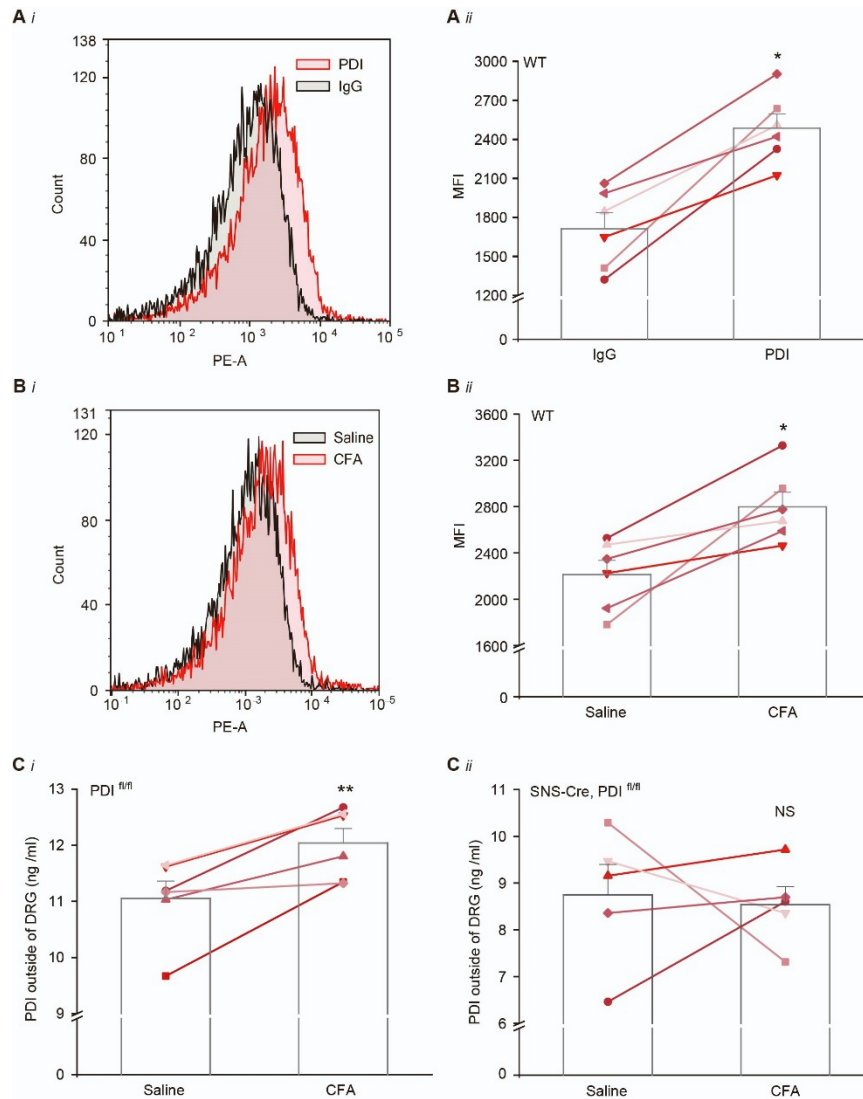
Figure S2. Secretion of PDI in DRG neurons is elevated in inflammatory pain condition. Related to Figure 1.

(A) Dissociated L3-L5 DRG cells were used for flow cytometry assay (FCM). Phycoerythrin conjugated PDI antibody was used for labeling PDI on DRG neuron surface, Phycoerythrin conjugated IgG was used as control. (Ai) Representative tracing of area under the traces (PE-A), which represents the counts of fluorescent positive cells. (Aii) Summary data of mean fluorescent intensity (MFI), which represents amount of PDI presents on surface of cells.

(B) Representative tracing (Bi) and summary data (Bii) of PE-A and MFI indicating PDI protein on surface of DRG cells dissociated from L3-L5 DRGs from mice subjected to CFA injection. L3-L5 DRGs were extracted on the 5th day after CFA injection. CFA treatment induced an increase of PDI on cell surface.

(C) ELISA assay of secreted PDI in the incubation solution bathing L3-L5 DRGs. Secreted PDI level was significantly increased in the L3-L5 DRGs of the PDI$^{fl/fl}$ mice (Ci) but not in the SNS-Cre,PDI$^{fl/fl}$ mice (Cii) on the 5th day after CFA injection. aired t test, $^*p < 0.05$, $^{**}p < 0.01$. Data are represented as mean ± SEM.
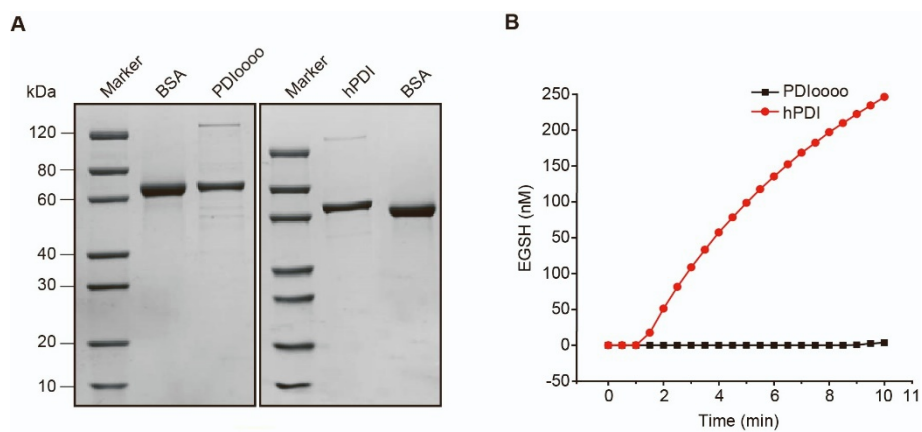
Figure S3. Preparation of recombinant hPDI and hPDIoooo. Related to Figure 2.

(A) Purity of hPDI was tested by SDS-PAGE.

(B) Enzymatic activity of purified hPDI and hPDIoooo was assessed by Di-E-GSSG assay, in which the content of reductive product EGSH acts as the indicator. .
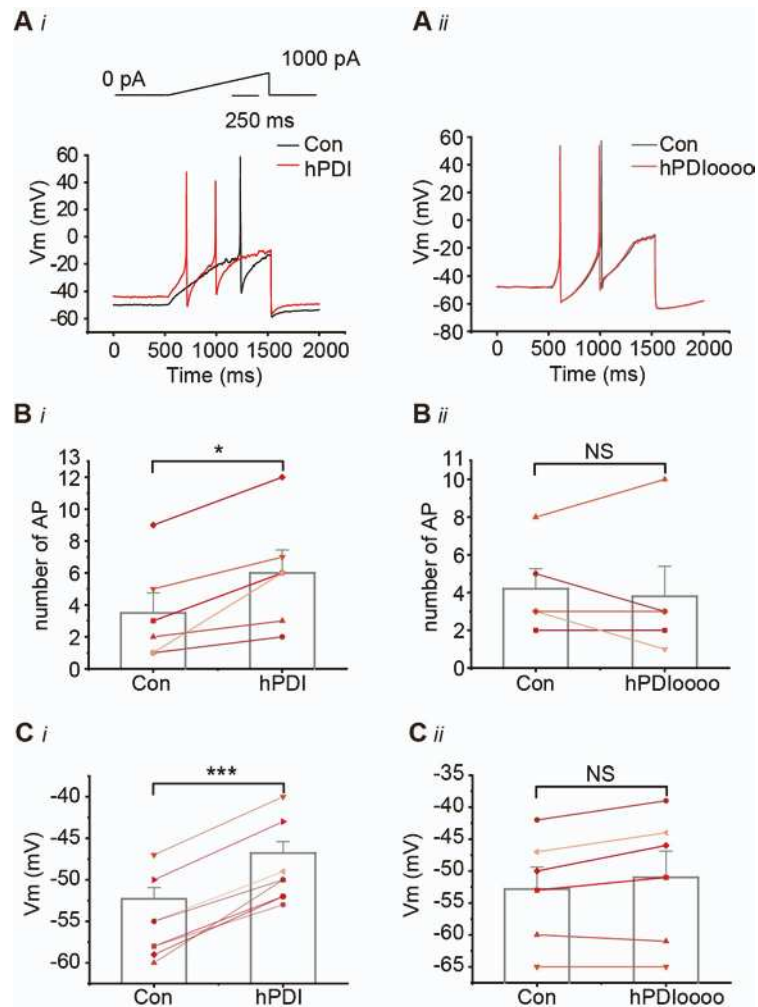
Figure S4. PDI increases firing of DRG neuron and depolarizes the cell membrane. Related to Figure 2.

(Ai and Aii) Exemplary recording of firing of action potential (AP) in DRG neurons. hPDI (100 nM) but not hPDIoooo (100 nM) increased firing of action potential (AP).

(Bi and Bii) Summary results of numbers of action potential evoked in DRG neurons before and after application of hPDI or hPDIoooo (Paired t test *$p < 0.05$).

(Ci and Cii) Summary results of the resting membrane potential of DRG neurons before and after application of hPDI or hPDIoooo (Paired t test, *$p < 0.05$). Data are represented as mean ± SEM.
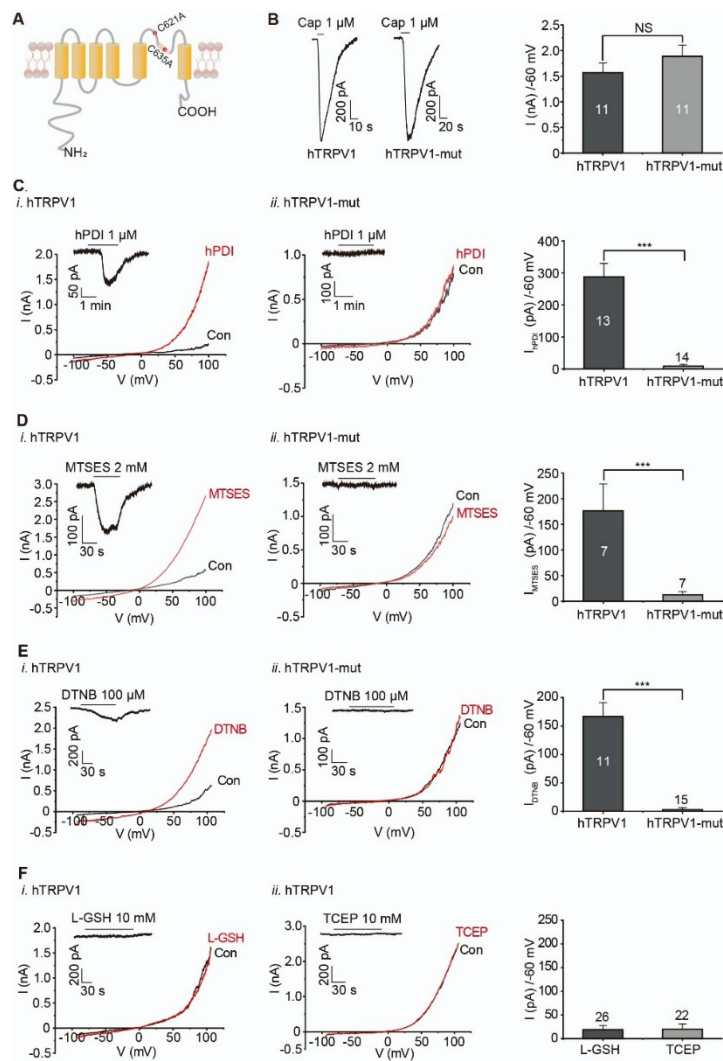
Figure S5. PDI and oxidants activate hTRPV1 through extracellular cysteine residues. Related to Figure 4.

(A) Topology diagram of human TRPV1 (hTRPV1) with the indicated mutated extracellular cysteines, C621A, C635A (hTRPV1-mut).

(B) Mutation of the extracellular cysteines did not affect capsaicin (Cap) –induced activation of hTRPV1 expressed in HEK293 cells. Exemplary and summarized hTRPV1 and hTRPV1-mut currents induced by Cap at holding potential of -60 mV were shown. NS, not significant (Student's t test, $p > 0.05$).

(C) Mutation of the extracellular cysteines abolished the hPDI-induced activation of hTRPV1 expressed in HEK 293 cells. Whole-cell currents of mTRPV1 and mTRPV1-mut were recorded either under a constant -60 mV holding potential (inset) or a ramp holding potential from -100 mV to +100 mV (800 ms). The current amplitudes recorded at -60 mV were summarized and analyzed.

(D-F) Exemplary and summarized hTRPV1 currents induced by the oxidants (MTSES, D), (DTNB, E) and the reductants (L-GSH, Fi), (TCEP, Fii). Mann-Whitney U test, *** $p < 0.001$. Numbers in bar graphs represent experimental repetitions. Data are represented as mean ± SEM.
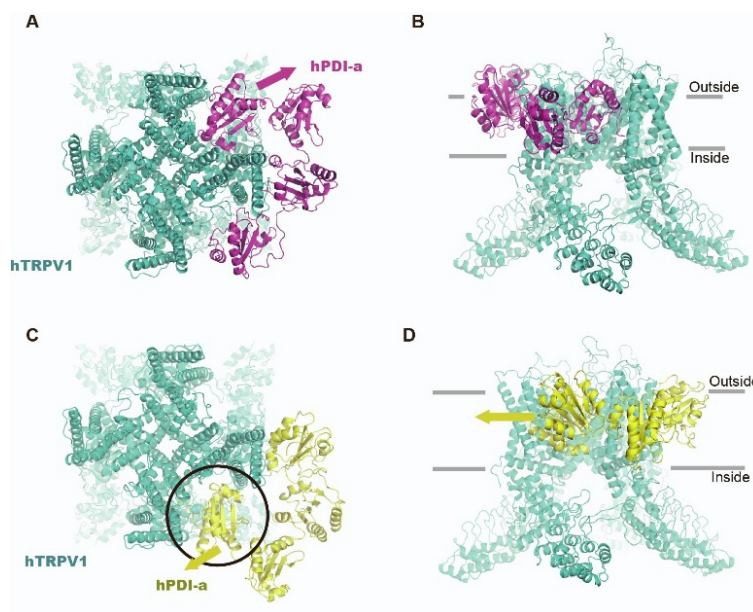
Figure S6. Structural simulation and molecular docking between hTRPV1 and hPDI. Related to Figure 5.

(A and B) Top view and side view of the interaction between hTRPV1 (cyan) and hPDI (purple). hTRPV1 structure is simulated based on rTRPV1 (PDB: 3j5p) and hPDI is in oxidation state (PDB: 4el1).

(C and D)Top view and side view of the interaction between hTRPV1 (cyan) and hPDI (yellow) which in reduced state (PDB : 4ekz).